Lorentz invariance violation and the *CPT*-odd electromagnetic response of a tilted anisotropic Weyl semimetal

Andrés Gómez[1,2,*] R. Martínez von Dossow[3,†] A. Martín-Ruiz[3,‡] and Luis F. Urrutia[3,§]

[1]*Facultad de Ciencias, Universidad Nacional Autónoma de México, 04510 Ciudad de México, México*
[2]*Institut für Theoretische Physik, Universität Heidelberg, Philosophenweg 16, 69120 Heidelberg, Germany*
[3]*Instituto de Ciencias Nucleares, Universidad Nacional Autónoma de México, 04510 Ciudad de México, México*

We derive the electromagnetic response of a particular fermionic sector in the minimal QED contribution to the Standard Model Extension (SME), which can be physically realized in terms of a model describing a tilted and anisotropic Weyl semimetal (WSM). The contact is made through the identification of the Dirac-like Hamiltonian resulting from the SME with that corresponding to the WSM in the linearized tight-binding approximation. We first calculate the effective action by computing the nonperturbative vacuum polarization tensor using thermal field theory techniques, focusing upon the corrections at finite chemical potential and zero temperature. Next, we confirm our results by a direct calculation of the anomalous Hall current within a chiral kinetic theory approach. In an ideal Dirac cone picture of the WSM (isotropic and nontilted) such response is known to be governed by axion electrodynamics, with the space-time dependent axion angle $\Theta(\boldsymbol{r}, t) = 2(\boldsymbol{b} \cdot \boldsymbol{r} - b_0 t)$, being $2\boldsymbol{b}$ and $2b_0$ the separation of the Weyl nodes in momentum and energy, respectively. In this paper we demonstrate that the node tilting and the anisotropies induce novel corrections at a finite density which however preserve the structure of the axionic field theory. We apply our results to the ideal Weyl semimetal $EuCd_2As_2$ and to the highly anisotropic and tilted monopnictide TaAs.

I. INTRODUCTION

The one loop effective action of QED in terms of external electromagnetic fields is a powerful tool to study multi-photon interactions at energies where the fundamental fermions are not excited, as well as transport properties arising from the resulting currents [1,2]. This action is obtained by "integrating" the fermions, yielding an effective Lagrangian which introduces additional contributions to the Maxwell term having the general form of a nonlinear electromagnetic response. A distinguished member of this class is the Euler-Heisenberg Lagrangian [3] which correctly anticipated some important results in QED, among which we find: (i) light-light scattering, as first discussed in Ref. [4] and subsequently given a full solution in Ref. [5];

(ii) pair-production from vacuum in an electric field, already noticed in [3] motivated in part from Ref. [6] and later given a complete description in [7]; and (iii) the need of charge renormalization, further developed in Refs. [8,9]. This effective Lagrangian is known to all orders in the electromagnetic field only in a restricted family of backgrounds, such as constant fields or plane wave fields, to name some well-known cases. For a review see for example [10]. The extension to the case of nonhomogeneous electromagnetic fields has remained a subject of investigation and several advances have been reported [11–15]. The inclusion of temperature and density, which is relevant to the study of transport properties in many body theory (e.g., metals, topological matter and quark-gluon plasma) and in spontaneously broken theories, has also been undertaken [16–24]. A recent review can be found in Ref. [25].

The advent of high power lasers together with increasingly energetic particle beams has fostered the theoretical and experimental interest in the general theory of quantum electrodynamics (QED) with intense background fields. Higher intensity, together with higher accuracy, demands an increase in the number of loops in the calculation and also to develop further nonperturbative methods. A detailed review of this whole topic, with emphasis on the advances in the last decade, is presented in Ref. [26]. Among the new

*andresgz@ciencias.unam.mx
†ricardo.martinez@correo.nucleares.unam.mx
‡alberto.martin@nucleares.unam.mx
§urrutia@nucleares.unam.mx

theoretical tools providing an alternative to the standard Feynman diagrams calculations, the semiclassical world-line instanton method, deriving from the "first quantized" approach to field theory, has proven particularly useful in the calculation of effective actions and related quantities in the study of QED processes in external fields [27,28].

Effective QED actions have been extensively studied in the framework of the Standard Model Extension (SME) [29,30]. This model parametrizes Lorentz invariance violations (LIV) in the fundamental interactions and by itself can be viewed as an effective model resulting from a more fundamental theory where this symmetry could be spontaneously broken by nonzero vacuum expectation values (VEVs) of tensorial operators. Contrary to the scalar Higgs field, such VEVs introduce fixed directions in space-time yielding the presumed violation. Such fixed tensors are coupled to the fields of the Standard Model providing all possible violating terms in the Lagrangian, consistent with the known symmetries of the fundamental interactions. These parameters must be extremely suppressed in order to find agreement with current experimental observations.

A relevant issue in this framework is to find relations among the actions characterizing a given sector of the model, in order to reduce the proliferation of coefficients which codify the LIV, as well as to understand the induced radiative corrections. This provides a natural setup for searching new effective electromagnetic actions arising from the additional couplings of the fermions to the electromagnetic field. A much studied particular case includes the *CPT*-odd violating terms in the fermion-photon sector of the minimal QED extension of the SME. There we find the modified Dirac action,

$$S_{\rm D} = \int d^4x \bar\Psi(x)\big(i\gamma^\mu\partial_\mu - \tilde b_\mu\gamma^5\gamma^\mu\big)\Psi(x), \qquad (1)$$

which includes the LIV coefficient $\tilde b^\mu$, together with the *CPT*-odd contribution to the photon sector

$$S_{\rm eff} = \frac{e^2}{32\pi^2}\int d^4x\,\Theta(x)\epsilon^{\alpha\beta\mu\nu}F_{\alpha\beta}F_{\mu\nu}, \qquad \Theta(x) = \tilde c_\mu x^\mu, \quad (2)$$

codified by another LIV coefficient $\tilde c_\mu$. Incidentally, the addition of (2) to the standard Maxwell action yields Carroll-Field-Jackiw (CFJ) electrodynamics [31], which can also be considered as a restricted version of axion electrodynamics [32,33] since the axion field Θ is not dynamical. The challenge here is to regain the action (2) through radiative corrections induced by the fermionic coupling in (1), which effectively amount to obtain the corresponding effective electromagnetic action. The conclusion is that in fact $\tilde c_\mu = \zeta\tilde b_\mu$, but with ζ being undetermined, having a finite value which depends on the regularization method. This was the subject of intense debate in the

literature as can be appreciated by the numerous references to the topic. A survey of the principal approaches regarding this issue can be found in Refs. [34–43]. Additional work yielding the effective one loop electromagnetic action induced by many of the additional LIV terms appearing in the fermionic sector of the minimal QED extension of the SME include nonperturbative [44–46] and perturbative calculations for some specific LIV parameters to first order [47–51], the inclusion of higher -derivative terms in the action [52–54], and higher order contributions of the LIV parameters in the one-loop effective action [55]. A review including these results is found in [56] and references therein.

Recently, a very interesting connection between the SME and the area of topological materials in condensed matter, where LIV occurs naturally, has been found through the identification of fermionic quasiparticles (excitations) of Dirac and/or Weyl-type in the linearized approximation of tight-binding Hamiltonians of topological phases of matter in regions close to the Fermi energy. Then, one can embed such Hamiltonians into a Dirac-Weyl field theory of the form (1) and subsequently apply the wealth of tools already developed in previous studies of LIV. In particular, the electromagnetic transport properties can be obtained through the calculation of the effective electromagnetic action, computed with standard methods in field theory. It is important to observe that, contrary to the case in high-energy physics, the LIV parameters that one identifies in such materials need not be highly suppressed, but are determined by their electronic structure and further subjected to experimental determination. In this way, the standard perturbative approach frequently used in most related calculations in high-energy physics, might prove inadequate in the condensed matter case, where nonperturbative methods could be required to obtain realistic results. Steps in this direction can be found in Refs. [57–62].

As we will show in the following, the use of quantum field theory methods can be particularly fruitful in the case of Weyl semimetals (WSMs), whose electronic Hamiltonians naturally include some of the LIV terms considered in the fermionic sector of the SME.

WSMs are topologically nontrivial conductors in which the valence and conduction bands touch at isolated points, (the so-called Weyl nodes) in the Brillouin zone, locally forming Dirac cones [63–65]. According to the Nielsen-Ninomiya theorem [66], the Weyl nodes in crystals occur in pairs of opposite chirality, indicating the presence of fermionic excitations of the Weyl-type. The individual nodes within a pair act as a source and sink of the Berry curvature, a topological property of the electronic Bloch wave functions. In this way the WSM phase is topologically protected by a nonzero Berry flux across the Fermi surface.

WSM phases in crystals require either broken spatial inversion symmetry or broken time-reversal symmetry,

or both. The Weyl phase with broken inversion symmetry has been predicted [67,68] and experimentally confirmed for the family of transition metal monopnictides compounds TaAs, NbAs, TaP, and NbP [69–75]. Those with broken time-reversal symmetry have been proposed for pyrochlore iridates $R_2Ir_2O_7$ (R is a rare-earth element) such as $Y_2Ir_2O_7$ [76–78].

In general, Weyl nodes in solids do not behave exactly in the same manner as their high-energy Lorentz invariant analogs because they are tilted and anisotropic. In a non-centrosymmetric WSM, for example, the Weyl nodes appear in pairs of opposite chirality, opposite tilting and rotated anisotropy. These deviations from the ideal Dirac cone picture influences several properties of WSMs like optical [75], spin texture [79], and expectedly, several anomalous transport phenomena.

There are a few common approaches for studying electronic transport in WSMs, including the Kubo formula [80], the chiral kinetic theory [81] and the loop effective action of quantum electrodynamics. In order to compare our results obtained within a quantum field theory approach we will use the chiral kinetic theory in this paper. This is a topologically modified semiclassical Boltzmann formalism (SBF) to describe the behavior of Weyl fermions at finite density. Within this approach, the many-electron system is described by a moving wave packet whose center satisfies semiclassical equations of motion augmented by an anomalous velocity term arising from the Berry curvature, which acts as a magnetic field in reciprocal space.

The relevance of the topological Berry curvature in the calculations of the transport properties, together with the presence of the Abelian-Pontryagin density as a factor in the effective action (2) arising from (1) has promoted the use of tools akin to anomaly calculations in field theory to obtain the effective action. Let us recall that the electromagnetic chiral anomaly is proportional to the Abelian-Pontryagin density whose integral is a topological invariant, thus suggesting that the topological properties ensuing from the Berry curvature in the SBF could be understood as a manifestation of the anomaly in the field theory approach. For example, using path integral methods the effective action (2) was obtained by introducing the electromagnetic coupling in Eq. (1) and subsequently eliminating the fermionic term proportional to $\tilde{b}_\mu$ through a chiral rotation. Nevertheless, instead of yielding a free fermionic action this produces an electromagnetic contribution arising from the nonzero Jacobian of the chiral transformation which is proportional to the Pontryagin density [82]. Following this idea, the Fujikawa prescription to obtain the chiral anomalies [83,84] has also been used to calculate the effective electromagnetic action of different materials in Refs. [85–87]. Nevertheless, as pointed out in Refs. [88–91] the anomaly does not incorporate all the parameters which one would expect to determine the full dynamics of the effective action. Also, the method of

eliminating the additional fermionic contributions via a chiral rotation cannot be easily extended to deal with the more complicated configurations envisaged in generalizations of the action (1). The reasons indicated above point to the need of presenting a full quantum-field theory method to obtain the required effective electromagnetic actions corresponding to fermionic systems described by such extensions. This is the purpose of this work. In particular, this procedure should clarify how the LIV corrections enter in the effective action, while the chiral anomaly remains insensitive to them, as mentioned above. As an application, this method will provide us with an alternative way to calculate the electromagnetic response of some particular cases in topological quantum matter.

In this work we consider the more general fermionic action,

$$S = \int d^4x \bar{\Psi}\left(\Gamma^\mu i\partial_\mu - M - e\Gamma^\mu A_\mu\right)\Psi, \qquad (3)$$

coupled to the electromagnetic field A_μ, and we restrict ourselves to

$$\Gamma^\mu = \gamma^\mu + c^\mu_{\ \nu}\gamma^\nu + d^\mu_{\ \nu}\gamma^5\gamma^\nu, \qquad M = a_\mu\gamma^\mu + b_\mu\gamma^5\gamma^\mu. \quad (4)$$

This corresponds to a particular choice of coefficients in the SME where we set $m = m_5 = H_{\mu\nu} = e_\mu = f_\mu = g_{\mu\nu\lambda} = 0$, in the notation of Table P52 of Ref. [92]. In Eq. (4), the matrices γ^μ are the standard ones and the isolated γ^μ contribution takes care of Lorentz covariant piece of the Dirac field. Also we have $\bar{\psi} = \psi^\dagger\gamma^0$. Our main motivation for this choice is that, close to the Fermi energy, the linear approximation of the tight-binding Hamiltonian of a WSM with two cones, having arbitrary tilting and anisotropy, can be embedded in the action (3). This will provide the opportunity to obtain the electromagnetic response from standard field theory methods via the effective action, as well as to compare these results with those obtained using the SBF. Also, we focus upon the *CPT*-odd contribution to the electromagnetic response since this sector describes novel and interesting phenomena such as the anomalous Hall effect and also provides contributions to the chiral magnetic effect. Since the conduction process strongly depends on the fermion filling of the valence and conduction bands we require to consider a finite particle density, which we achieve by introducing the chemical potential at zero temperature as a first approximation.

Aside from further detailing the calculations in our previous results [61], together with extending them to the anisotropic case, our aim in this work is to make the first steps in establishing the relation between the two alternative methods considered; the effective action calculation and the semiclassical Boltzmann formalism. This might shed additional light in the role that the chiral anomaly plays in the characterization of the electromagnetic

transport properties of WSMs in the framework of the effective action.

The paper is organized as follows. In Sec. II we define the general effective electromagnetic action and consider only the restriction to the *CPT*-odd contribution of the vacuum polarization tensor $\Pi^{\mu\nu}$, which we relate to the resulting axionic electrodynamics describing the response of the medium we study. The action to be integrated in the presence of an external electromagnetic field is selected from the fermionic sector of the SME with the choices indicated in Eq. (4) and turns out to be chiral. The detailed decomposition of the full vertices and propagators into their chiral contributions, labeled by $\chi = \pm 1$, is carried in Sec. II A together with Appendix A. In this way, the vacuum polarization tensor is split into two contributions, $\Pi_\chi^{\mu\nu}$, whose expressions are analogous and are calculated in Sec. II B with the help of the Appendix B. The condensed matter Hamiltonian describing a tilted anisotropic WSM, whose electromagnetic response is obtained as an application of the previous results, is introduced in Sec. III. We show how to embed this Hamiltonian in the fermionic action (4) and write the relations among their parameters. To calculate the effective current we incorporate the finite density regime via the chemical potential μ at zero temperature, which is introduced in Sec. IV using the Matsubara prescription. The calculation is further split into a μ-independent contribution, calculated in Sec. IV A plus the Appendix C, together with a μ-dependent piece, carrying all the information regarding the tilting and anisotropy, which is summarized in Sec. IV B and heavily relies on the Appendixes D–F. Section V is devoted to the calculation of the anomalous Hall current using the kinetic theory approach, as a way of comparing the effective action results with a well-established and powerful method in condensed matter physics. Some applications of the matching results focusing on the anomalous Hall current are described in Sec. VI using EuCd$_2$As$_2$ and TaAs, which are well-known tilted and anisotropic WSMs. Finally we close in Sec. VII with the summary and results. Our metric convention is $\eta_{\mu\nu} = \mathrm{diag}(1, -1, -1, -1)$ and $\epsilon^{0123} = +1$.

II. THE EFFECTIVE ACTION

Let us start from the action (3) together with the selection (4) for Γ^μ and M. We are interested in a low-energy regime where the fermions are not excited, yielding an effective contribution to the electromagnetic interaction allowing the determination of the induced current. To this end we calculate the effective action $S_{\mathrm{eff}}(A)$ given by

$$
\begin{aligned}
&\exp[iS_{\mathrm{eff}}(A)] \\
&= \int D\bar{\Psi}D\Psi \exp\left[i\int d^4x \bar{\Psi}(\Gamma^\mu i\partial_\mu - M - e\Gamma^\mu A_\mu)\Psi\right] \\
&= \det(\Gamma^\mu i\partial_\mu - M - e\Gamma^\mu A_\mu).
\end{aligned}
\tag{5}
$$

Following the standard procedure we introduce the non-interacting Green function $S = i/(i\Gamma^\mu\partial_\mu - M)$ and we write

$$
\begin{aligned}
\det(i\Gamma^\mu\partial_\mu - M - e\Gamma^\mu A_\mu) &= \det(\Gamma^\mu i\partial_\mu - M) \\
&\times \det[1 - S\Gamma^\alpha(-ieA_\alpha)].
\end{aligned}
\tag{6}
$$

Discarding the irrelevant normalization factor $\det(i\Gamma^\mu\partial_\mu - M)$, using the identity $\det M = \exp\mathrm{Tr}\ln M$ and the power expansion of the logarithm we solve S_{eff} from Eq. (5) obtaining

$$
iS_{\mathrm{eff}}(A) = \mathrm{Tr}\sum_{n=1}^\infty -\frac{1}{n}\left[S(-ie\Gamma^\alpha A_\alpha)\right]^n.
\tag{7}
$$

The trace Tr is taken in coordinate as well as in matrix space, while tr is reserved to the trace in matrix space. To second order in A_α we obtain

$$
\begin{aligned}
iS_{\mathrm{eff}}^{(2)}(A) = \frac{e^2}{2}\int d^4x d^4x' A_\mu(x')\mathrm{tr} \\
\times [S(x-x')\Gamma^\mu S(x'-x)\Gamma^\nu]A_\nu(x),
\end{aligned}
\tag{8}
$$

in coordinate space. Going to the Fourier space, with the conventions

$$
\begin{aligned}
A_\nu(x) &= \int \frac{d^4k}{(2\pi)^4} e^{-ikx} A_\nu(k), \\
S(x-x') &= \int \frac{d^4k}{(2\pi)^4} e^{-ik(x-x')} S(k), \qquad i\partial_\mu = k_\mu,
\end{aligned}
\tag{9}
$$

yielding

$$
S(k) = \frac{i}{\Gamma^\mu k_\mu - M},
\tag{10}
$$

we recast Eq. (8) as

$$
\begin{aligned}
iS_{\mathrm{eff}}^{(2)}(A) = +\frac{e^2}{2}\int \frac{d^4p}{(2\pi)^4} A_\mu(-p)\left[\int \frac{d^4k}{(2\pi)^4}\mathrm{tr}[S(k-p)\right. \\
\left. \times \Gamma^\mu S(k)\Gamma^\nu]\right]A_\nu(p).
\end{aligned}
\tag{11}
$$

Let us introduce the vacuum polarization tensor $\Pi^{\mu\nu}(p)$

$$
i\Pi^{\mu\nu}(p) = e^2\left[\int \frac{d^4k}{(2\pi)^4}\mathrm{tr}[S(k-p)\Gamma^\mu S(k)\Gamma^\nu]\right],
\tag{12}
$$

which produces the final expression for the effective action

$$S_{\text{eff}}^{(2)}(A) = \frac{1}{2} \int \frac{d^4 p}{(2\pi)^4} A_\mu(-p) \Pi^{\mu\nu}(p) A_\nu(p), \quad (13)$$

Since $S_{\text{eff}}^{(2)}$ is real we must have $\Pi_{\mu\nu}^*(p) = \Pi_{\nu\mu}(p)$.

In the following we consider only the *CPT*-odd contribution to the effective action (13) which, as we will show, keeps the form of Eq. (2) with a new vector $\mathcal{B}_\lambda$ to be determined, which replaces the original $\tilde{c}_\lambda$. The resulting vacuum polarization contribution together with the new axion field is

$$\Pi^{\mu\nu}(p) = -i\frac{e^2}{2\pi^2}\mathcal{B}_\lambda p_\kappa \epsilon^{\mu\nu\lambda\kappa}, \qquad \Theta(x) = 2\mathcal{B}_\lambda x^\lambda. \quad (14)$$

In other words, the LIV parameters of the model $c_{\mu\nu}, d_{\mu\nu}, a_\mu, b_\mu$ will contribute only through the vector $\mathcal{B}_\lambda$ yielding the full electromagnetic action (in Gaussian units),

$$S[A_\mu] = \int d^4x \left[-\frac{1}{16\pi}F_{\mu\nu}F^{\mu\nu} - \frac{1}{c}J^\mu A_\mu + \frac{\alpha}{16\pi^2}\Theta(x)F_{\mu\nu}\tilde{F}^{\mu\nu} \right], \quad (15)$$

where the electromagnetic tensor is $F_{\mu\nu} = \partial_\mu A_\nu - \partial_\nu A_\mu$, with its dual $\tilde{F}^{\mu\nu} = \frac{1}{2}\epsilon^{\mu\nu\alpha\beta}F_{\alpha\beta}$, and $\alpha = e^2/(\hbar c)$ is the fine structure constant. The resulting equations of motion are

$$\partial_\mu F^{\mu\nu} = \frac{4\pi}{c}J^\mu + \frac{\alpha}{\pi}(\partial_\mu\Theta)\tilde{F}^{\mu\nu}. \quad (16)$$

Following the conventions of Ref. [93], we have

$$\boldsymbol{\nabla} \cdot \mathbf{E} = 4\pi\rho + \frac{\alpha}{\pi}(\boldsymbol{\nabla}\Theta) \cdot \mathbf{B},$$

$$\boldsymbol{\nabla} \times \mathbf{B} - \frac{1}{c}\frac{\partial\mathbf{E}}{\partial t} = \frac{4\pi}{c}\mathbf{J} - \frac{\alpha}{\pi}\frac{1}{c}\frac{\partial\Theta}{\partial t}\mathbf{B} - \frac{\alpha}{\pi}(\boldsymbol{\nabla}\Theta) \times \mathbf{E}, \quad (17)$$

in terms of the electromagnetic fields. Equation (17) yield the effective current densities

$$\rho_{\text{eff}} = \frac{\alpha}{4\pi^2}(\boldsymbol{\nabla}\Theta) \cdot \mathbf{B}, \qquad \mathbf{J}_{\text{eff}} = -\frac{c\alpha}{4\pi^2}\left(\frac{\partial\Theta}{\partial x^0}\mathbf{B} + (\boldsymbol{\nabla}\Theta) \times \mathbf{E}\right). \quad (18)$$

which provide a realization of the magnetoelectric effect. From the homogeneous Maxwell's equations $\partial_\mu\tilde{F}^{\mu\nu} = 0$ one can verify the effective charge conservation $\partial_t\rho_{\text{eff}} + \boldsymbol{\nabla} \cdot \mathbf{J}_{\text{eff}} = 0$ for an arbitrary coordinate dependent axion field $\Theta(x)$. Equation (18) can be written in terms of $\mathcal{B}_0 = \partial_0\Theta/2$ and $\boldsymbol{\mathcal{B}} = \{\mathcal{B}^i\}$, with $= \mathcal{B}_i = -\mathcal{B}^i = \partial_i\Theta/2$. The current $\mathbf{J}_{\text{AHE}} = (c\alpha/2\pi^2)\boldsymbol{\mathcal{B}} \times \mathbf{E}$ describes the anomalous Hall effect, while $\mathbf{J}_{\text{CME}} = -(\alpha/2\pi^2)\mathcal{B}_0\mathbf{B}$ contributes to the chiral magnetic effect. In the following we set $\hbar = c = 1$ so that $\alpha = e^2 = 1/137$.

A. The chiral propagators

Now we give some preliminary steps for the calculation of the vacuum polarization tensor. In the absence of the unit matrix, our generalized Dirac operator $\Gamma^\mu k_\mu - M$, in Eq. (4), is linear in γ^μ and $\gamma^5\gamma^\mu$. The appearance of the matrix γ^5 suggests the convenience of using left and right chiral projectors in order to replace γ^5 by its eigenvalues ± 1. This procedure was first performed in Ref. [39] and subsequently used in Refs. [89,94], among others. Therefore, it is convenient to define the operators,

$$P_\chi = \frac{1 + \chi\gamma^5}{2}, \qquad \gamma_5^2 = 1, \qquad P_+ + P_- = 1,$$
$$P_\chi^2 = P_\chi, \qquad P_+P_- = P_-P_+ = 0, \quad (19)$$

which project onto the right-handed (R) and the left-handed (L) subspace, with $\chi = +1$ and $\chi = -1$, respectively. Note that $\gamma^\mu P_\chi = P_{-\chi}\gamma^\mu$. The projectors (19) allows us to define the matrices Γ_χ^μ such that

$$\Gamma^\mu P_\chi = (\delta^\mu{}_\nu + c^\mu{}_\nu - \chi d^\mu{}_\nu)\gamma^\nu P_\chi \equiv \Gamma_\chi^\mu P_\chi, \quad (20)$$

which explicitly identifies

$$\Gamma_\chi^\mu = (m_\chi)^\mu{}_\nu\gamma^\nu, \qquad (m_\chi)^\mu{}_\nu = \delta^\mu{}_\nu + c^\mu{}_\nu - \chi d^\mu{}_\nu. \quad (21)$$

The apparent mismatch that $(m_\chi)^\mu{}_\nu$ gets a $-\chi$ factor in front of $d^\mu{}_\nu$ is readily clarified recalling that in our conventions we have $\gamma^5\gamma^\mu P_\chi = -\gamma^\mu\gamma^5 P_\chi = -(\chi)\gamma^\mu P_\chi$. In the following we indistinctly use the notation $\chi = (+1, -1)$ or $\chi = (R, L)$.

To proceed forward with the calculation we now split the combination $T^{\mu\nu}(k, p) = S(k-p)\Gamma^\mu S(k)\Gamma^\nu$ inside the trace of $\Pi^{\mu\nu}(p)$ in Eq. (12) into its left- and right-handed parts, i.e.,

$$T_\chi^{\mu\nu}(k, p) = S(k-p)\Gamma^\mu S(k)\Gamma^\nu P_\chi, \quad (22)$$

which implies that the vacuum polarization can be written as the sum $\Pi^{\mu\nu}(p) = \Pi_L^{\mu\nu}(p) + \Pi_R^{\mu\nu}(p)$, with

$$i\Pi_\chi^{\mu\nu}(p) = e^2 \int \frac{d^4k}{(2\pi)^4} \text{tr}\left[T_\chi^{\mu\nu}(k, p)\right] \quad (23)$$

being the vacuum polarization of a massless fermion with chirality χ.

The next step is to calculate $S(k)\Gamma^\nu P_\chi$, with $S(k)$ given in Eq. (10). The Γ^ν in the numerator changes into a linear combination of standard matrices γ^α according to Eq. (20), but we are still left with $S(k)\gamma^\alpha P_\chi$ where we require to determine the action of the projector in the denominator of the propagator. This is done in the Appendix A with the results

$$\frac{i}{\Gamma^\mu k_\mu - M} \gamma^\alpha P_\chi = P_\chi S_\chi(k) \gamma^\alpha,$$

$$S_\chi(k) = \frac{i}{\left(k_\mu (m_\chi)^\mu{}_\nu - (C_\chi)_\nu\right)\gamma^\nu},$$

$$(C_\chi)_\nu = a_\nu - \chi b_\nu. \tag{24}$$

Note that the propagators S_χ, having the generic form $i/(Z_\nu \gamma^\nu)$, can be readily rationalized as $i(Z_\nu \gamma^\nu)/Z^2$.

B. The vacuum polarization tensor

We now concentrate in the calculation of each contribution $\Pi^{\mu\nu}_\chi(p)$. Inserting Eqs. (12) and (24) into (22) and (23) and using the cyclic property of the trace we have

$$i\Pi^{\mu\nu}_\chi(p) = e^2 (m_\chi)^\mu{}_\beta (m_\chi)^\nu{}_\alpha$$
$$\times \int \frac{d^4 k}{(2\pi)^4} \mathrm{tr}\left[S_\chi(k-p)\gamma^\beta S_\chi(k)\gamma^\alpha P_\chi\right]. \tag{25}$$

Having in mind the application of our results to the transport properties of WSMs, in the following we restrict ourselves to the *CPT*-odd (axial) contributions $\Pi^{\mu\nu}_{A,\chi}$ of the vacuum polarization, which are obtained by selecting the terms $\chi\gamma^5/2$ in the projector P_χ of Eq. (25). Then we are left with

$$i\Pi^{\mu\nu}_{A,\chi}(p) = \frac{\chi}{2} e^2 (m_\chi)^\mu{}_\beta (m_\chi)^\nu{}_\alpha$$
$$\times \int \frac{d^4 k}{(2\pi)^4} \mathrm{tr}\left[S_\chi(k-p)\gamma^\beta S_\chi(k)\gamma^\alpha \gamma^5\right]. \tag{26}$$

Clearly, the full-axial contribution to the vacuum polarization is the sum of the L and R parts, i.e., $\Pi^{\mu\nu}_A = \Pi^{\mu\nu}_{A,L} + \Pi^{\mu\nu}_{A,R}$. The calculation indicated in Eq. (26) is presented in the Appendix B with the result

$$\Pi^{\mu\nu}_{A,\chi}(p) = -2\chi e^2 (\det m_\chi)(m_\chi^{-1})^\rho{}_\lambda \epsilon^{\mu\nu\lambda\kappa} p_\kappa I^\chi_\rho(C), \tag{27}$$

with

$$I^\chi_\rho(C) = \int \frac{d^4 k}{(2\pi)^4} g^\chi_\rho(k_0, \boldsymbol{k}), \qquad g^\chi_\rho(k_0, \boldsymbol{k}) = \frac{(k'_\chi - C_\chi)_\rho}{[(k'_\chi - C_\chi)^2]^2}, \tag{28}$$

where we have taken that $(k'_\chi)_\mu = k_\alpha (m_\chi)^\alpha{}_\mu$. Previous to regularization, the above expression is our final result for the vacuum polarization in Minkowski spacetime. The result (27) holds for arbitrary LIV parameters $c^\mu{}_\nu$, $d^\mu{}_\nu$, a_μ, and b_μ as long as these produce invertible matrices $(m_\chi)^\mu{}_\nu$. Note that this result is nonperturbative in these parameters. From Eqs. (14) and (27) we can read the chiral

contributions to $\mathcal{B}_\lambda = \mathcal{B}^+_\lambda + \mathcal{B}^-_\lambda$ as

$$\mathcal{B}^\chi_\lambda = -i4\pi^2 \chi (\det m_\chi)(m_\chi^{-1})^\rho{}_\lambda I^\chi_\rho(C). \tag{29}$$

III. THE MODEL

In order to further motivate the additional choices we make to obtain our final result for $\mathcal{B}_\mu$ which will determine the electromagnetic response (18), we introduce a simple model of a WSM consisting of two Weyl nodes of opposite chiralities separated in momentum and energy, ignoring the nonuniversal corrections due to band bending far away from the nodes. The low-energy Hamiltonian for a Weyl node with chirality χ can be expressed as

$$H_\chi(\boldsymbol{k}) = \boldsymbol{v}_\chi \cdot (\boldsymbol{k} + \chi\tilde{\boldsymbol{b}})\sigma_0 - \chi\tilde{b}_0 \sigma_0 + \chi(\boldsymbol{k} + \chi\tilde{\boldsymbol{b}})\mathbb{A}_\chi \boldsymbol{\sigma},$$
$$\boldsymbol{W}\mathbb{A}_\chi \boldsymbol{\sigma} \equiv W^i A_{\chi ij}\boldsymbol{\sigma}^j, \tag{30}$$

where $\boldsymbol{k}$ is the crystal momentum, $\boldsymbol{\sigma}$ is the vector of Pauli spin matrices, σ_0 is the 2×2 unit matrix, and W^i denotes an arbitrary vector. This model describes two Weyl nodes located at $-\chi\tilde{\boldsymbol{b}}$ $(-\chi\tilde{b}_0)$ in momentum (energy) with respect to the origin at $\boldsymbol{k} = \boldsymbol{0}$ (the zero-energy plane). The tilting velocity of each cone is $\boldsymbol{v}_\chi = \{v^i_\chi\}$ and $\mathbb{A}_\chi = [(A_\chi)_{ij}]$ is the matrix of anisotropic Fermi velocities, with the notation indicated in the second term of Eq. (30).

The dispersion relation of this model is

$$E_{s\chi}(\boldsymbol{k}) = -\chi\tilde{b}_0 + \boldsymbol{\mathcal{V}}_\chi \cdot \boldsymbol{\mathcal{K}}_\chi + s\mathcal{K}_\chi, \tag{31}$$

where $s = \pm 1$ is the band index, $\boldsymbol{\mathcal{V}}_\chi = \mathbb{A}^{-1}_\chi \boldsymbol{v}_\chi$, $\boldsymbol{\mathcal{K}}_\chi = (\boldsymbol{k} + \chi\tilde{\boldsymbol{b}})\mathbb{A}_\chi$, and $\mathcal{K}_\chi = |\boldsymbol{\mathcal{K}}_\chi|$. In order to illustrate the emergence of the linearly dispersing model we are considering in Eq. (30), the left panel of Fig. 1 shows a general energy dispersion for a two-node Weyl semimetal, including band bending far away from the nodes described by a more general tight-binding Hamiltonian. When the Fermi level is close to the band crossings, this Hamiltonian can be linearized around each node, yielding to our model of Eq. (30). In the middle panel of Fig. 1 we show the Weyl cones without tilting and with isotropic Fermi velocity. The right panel displays tilted Weyl cones with anisotropic Fermi velocity.

An important step in our calculation is the identification of the parameters in the condensed matter Hamiltonian (30) with the parameters entering the free Hamiltonian, i.e., without the electromagnetic coupling, resulting from the fermionic action (3) in the SME. These relations allow us to express the results obtained from the effective action in Sec. II, in terms of the physical parameters characterizing the WSM. To facilitate this identification we rewrite (30) as

$$H_L(\boldsymbol{k}) = \boldsymbol{v}_L \cdot \boldsymbol{k} - \boldsymbol{v}_L \cdot \tilde{\boldsymbol{b}} + \tilde{b}_0 - \boldsymbol{k}\mathbb{A}_L \boldsymbol{\sigma} + \tilde{\boldsymbol{b}}\mathbb{A}_L \boldsymbol{\sigma}, \tag{32}$$
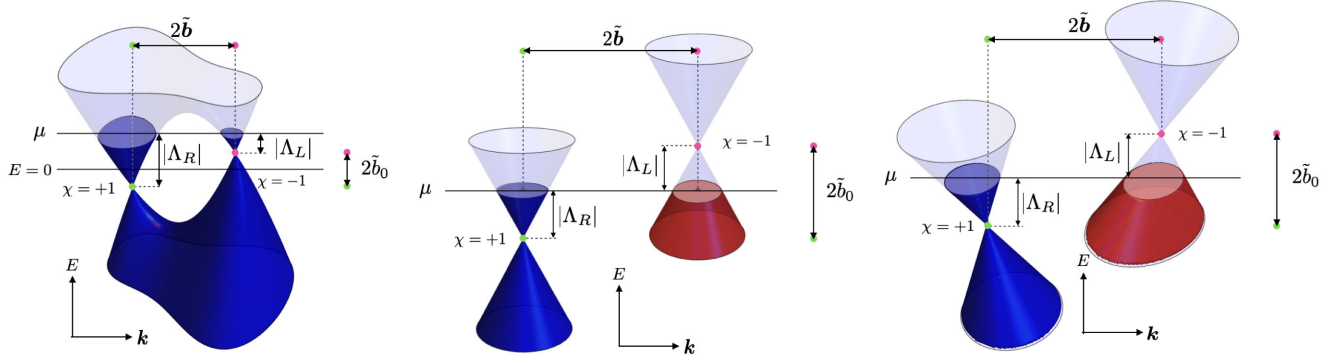
FIG. 1.   Left: energy dispersion for a two-node WSM including band bending far away from the nodes. Middle: low-energy spectrum of a two-node WSM without tilting and with isotropic Fermi velocity. Right: low-energy spectrum of a two-node tilted Weyl cones with anisotropic Fermi velocity. The black line represents the position of the Fermi level μ and $\Lambda_\chi = \mu + \chi\tilde{b}_0$ measures the band filling.

$$H_R(\mathbf{k}) = \mathbf{v}_R \cdot \mathbf{k} + \mathbf{v}_R \cdot \tilde{\mathbf{b}} - \tilde{b}_0 + \mathbf{k}\mathbb{A}_R\boldsymbol{\sigma} + \tilde{\mathbf{b}}\mathbb{A}_R\boldsymbol{\sigma}, \quad (33)$$

where R, L denotes the chiralities $\chi = +, -$ respectively, as indicated previously. Note that in this Hamiltonian there are 32 independent parameters contained in $\chi\tilde{\mathbf{b}}$, χb_0, $\mathbf{v}_\chi$, and $\mathbb{A}_\chi$.

To accomplish this task we now focus on the fermionic system described by the extended Dirac operator $(\Gamma^\mu i\partial_\mu - M)$ with the specific choices in Eq. (4), which account for 40 independent parameters. A convenient simplification in the construction of the Dirac-Hamiltonian is to set $\Gamma^0 = \gamma^0$, which demands $c^0{}_\nu = 0$ and $d^0{}_\nu = 0$. This cuts down the number of independent parameters in the SME to the required $40 - 8 = 32$ and yields the Hamiltonian

$$\mathcal{H} = \gamma^0\Gamma^k i\partial_k + \gamma^0 M. \quad (34)$$

In the chiral representation of the gamma matrices, where σ_0 is the 2×2 unit matrix and σ^i are the standard Pauli matrices, we have

$$\gamma^0 = \begin{pmatrix} 0 & \sigma_0 \\ \sigma_0 & 0 \end{pmatrix}, \qquad \gamma^i = \begin{pmatrix} 0 & \sigma^i \\ -\sigma^i & 0 \end{pmatrix},$$

$$\gamma^5 = \begin{pmatrix} -\sigma_0 & 0 \\ 0 & \sigma_0 \end{pmatrix}, \quad (35)$$

and $\mathcal{H}$ separates into right (R) and left (L) contributions according to the chiral projectors (19). Before writing them

explicitly it is convenient to introduce the additional parametrization

$$\delta^\mu{}_\nu + c^\mu{}_\nu - \chi d^\mu{}_\nu = (m_\chi)^\mu{}_\nu \equiv \begin{pmatrix} 1 & 0 \\ V^i_\chi & (U_\chi)^i{}_j \end{pmatrix}, \quad (36)$$

which arises from the choice $\Gamma^0 = \gamma^0$. A direct calculation shows,

$$\mathcal{H}_L = -V^i_L k_i + k_i(U_L)^i{}_j\sigma^j + C_{L0} - C_{Lj}\sigma^j, \quad (37)$$

$$\mathcal{H}_R = -V^i_R k_i - k_i(U_R)^i{}_j\sigma^j + C_{R0} + C_{Rj}\sigma^j. \quad (38)$$

For further clarity, let us recap the steps we have followed: we start with the parameters $c^\mu{}_\nu$, $d^\mu{}_\nu$, a_μ, and b_μ in the SME, then the chiral representation naturally introduces $(m_\chi)^\mu{}_\nu$ and $(C_\chi)_\nu$ according to (21) and (24). To fulfill the restriction $\Gamma^0 = \gamma^0$ we have further introduced V^i_χ and $(U_\chi)^i{}_j$ in $(m_\chi)^\mu{}_\nu$ as defined in Eq. (36). Summarizing, at this stage the SME parametrization of the Hamiltonian $\mathcal{H}$ is presented in terms of V^i_χ, $(U_\chi)^i{}_j$, $(C_\chi)_\mu$, with $\chi = \pm 1$.

The final step is to write the parameters of the SME Hamiltonian (34) in terms of those in the condensed matter Hamiltonian (30), i.e., to identify Eq. (32) with Eq. (37) and Eq. (33) with Eq. (38). We obtain the following relations:

$$\begin{aligned}
(m_\chi)^i{}_0 &= V^i_\chi = v^i_\chi, & (m_\chi)^i{}_j &= (U_\chi)^i{}_j = (A_\chi)_{ij}, \\
(C_\chi)_0 &= \chi(v^i_\chi \tilde{b}^i - \tilde{b}_0), & (C_\chi)_j &= \chi\tilde{b}^i(A_\chi)_{ij}, \\
a_0 &= \frac{1}{2}\tilde{b}^i(v^i_R - v^i_L), & b_0 &= \tilde{b}_0 - \frac{1}{2}\tilde{b}^i(v^i_R + v^i_L), \\
a_j &= \frac{1}{2}\tilde{b}^i[(A_R)_{ij} - (A_L)_{ij}], & b_j &= -\frac{1}{2}\tilde{b}^i[(A_R)_{ij} + (A_L)_{ij}].
\end{aligned} \quad (39)$$

IV. THE FINITE DENSITY REGIME

In order to apply the results of our effective action calculation in Sec. II to obtain the conduction current produced by the WSM characterized by the Hamiltonian (30) in the zero temperature limit, we have to incorporate the effects of the chemical potential μ because its location will determine the filling of the conduction and the valence bands of each node, thus yielding the conductivity. To this end we choose the Matsubara imaginary-time formalism to correctly incorporate the μ-dependence in the effective action [19,20], which we implement through the substitution [21–23],

$$\int \frac{d^4k}{(2\pi)^4} \to \left(\int \frac{d^4k}{(2\pi)^4} \right)_{T=0,\mu=0} + iT \sum_{n=-\infty}^{\infty} \int \frac{d^3\boldsymbol{k}}{(2\pi)^3}, \quad (40)$$

in Eq. (28). Here $k_0 \to k_0 = i\omega_n + \mu$ and the sum in Eq. (40) is over the Matsubara frequencies $\omega_n = (2n+1)\pi T$ required to produce antiperiodic boundary conditions for the fermions [20]. We think of the prescription (40) as a natural regulator for potentially divergent contributions.

Since we are dealing with chiral fermionic excitations whose dispersion behaves linearly around the Weyl nodes we have to locate the chemical potential close to the nodes in order for the approximation to be valid. Once we do this, the calculation will tell us which band (valence or conduction) in each node contributes to the conduction process. Let us recall that completely filled bands do not contribute to the current, which is due only to the partially filled bands.

Next we focus on Eq. (28) and make use of the following relation to evaluate the contribution of the chemical potential at zero temperature [19],

$$\lim_{T\to 0} T \sum_{n=-\infty}^{\infty} g_\rho^\chi(k_0 = i\omega_n + \mu, \boldsymbol{k}) = \sum_{\mathrm{Re}(k_0^{\chi\#})<\mu} \mathrm{Res}\big[g_\rho^\chi(k_0, \boldsymbol{k})\big], \quad (41)$$

where $k_0^{\chi\#}$ stand for the location of the poles in k_0 of $g_\rho(k_0, \boldsymbol{k})$, with "Res" denoting the corresponding residue. The sum is made over all the existing poles having a real part less than the chemical potential.

Next we split $I_\rho^\chi(C) = I_\rho^{\chi(1)}(C) + I_\rho^{\chi(2)}(C)$, where the superindex (1) refers to the μ-independent contribution, while the superindex (2) labels the μ-dependent piece. In turn, this says that $\mathcal{B}_\mu = \mathcal{B}_\mu^{(1)} + \mathcal{B}_\mu^{(2)}$.

A. The μ-independent contribution

This term reduces to the standard zero-temperature, zero-chemical potential piece, which has been previously obtained in the literature [82,85]. Going back to Eq. (28), this corresponds to the direct evaluation of the integral $I_\rho(C)$

after the change of integration variables $k'_\mu = k_\nu m^\nu_{\ \mu}$. Since the only vector at our disposal is C_μ, we have

$$I_\rho^{\chi(1)}(C_\chi) = \frac{i}{(\det m_\chi)} N_\chi (C_\chi)_\rho,$$

$$N_\chi = \frac{1}{C_\chi^2} \left[\int \frac{d^4k'}{(2\pi)^4} \frac{(k'-C_\chi)\cdot C_\chi}{[(k'-C_\chi)^2]^2} \right]_E, \quad (42)$$

where the integral inside the square brackets is in Euclidean space and the factor $+i$ comes from the Wick rotation. The factor N_χ is regularization dependent and could only be a function of the magnitude of the four-vector $(C_\chi)_\mu$. However, a change of scale $C_\sigma \to \lambda C_\sigma$ followed by an additional change of variables $k''_\mu = \lambda k'_\mu$ shows that N_χ is just a numerical factor, independent of $(C_\chi)_\mu$. Therefore, N_χ is the same for both left- and right-handed excitations, i.e., $N_\chi = N$. In this way, the total contribution to the vacuum polarization in this case is summarized in the vector,

$$\mathcal{B}_\lambda^{(1)} = 4\pi^2 N \sum_{\chi=\pm 1} \chi (C_\chi)_\rho (m_\chi^{-1})^\rho_{\ \lambda}, \quad (43)$$

according to Eq. (14). As shown previously in the literature the factor N is finite but undetermined [34–43]. Its dependence upon the regularization procedure has been studied in Ref. [85] and the final choice is made by selecting an observable quantity predicted by the model. In our case we take the anomalous Hall conductivity $\sigma_{xy} = -e^2 \tilde{b}_z/(2\pi)^2$ as the quantity to be predicted in the isotropic zero-tilting limit, which results by selecting $N = -1/(8\pi^2)$ [85]. The method that we employ to regularize the integral (42), yielding the chosen value for the coefficient N, requires to take a cutoff in the direction of $(C_\chi)_\rho$ and involves performing a direct integration in cylindrical coordinates. Without loss of generality, we assume that the vector $\boldsymbol{C}_\chi$ has only a component along the z-axis, such that we can conveniently split $\mathbf{k}' = \mathbf{k}'_z + \mathbf{k}'_\perp$. As suggested in Ref. [38], we rely on the residual rotational symmetry in the plane perpendicular to $\mathbf{C}_\chi$ to perform first the integrations over $k'_\perp$ and ϕ. Thus, the integral (42) turns out to be

$$N = \frac{1}{C_\chi^2 (2\pi)^4} \int_{-\infty}^{\infty} dk'_0 \int_{-\infty}^{\infty} dk'_z \int_0^{2\pi} d\phi \int_0^{\infty} dk'_\perp k'_\perp$$

$$\times \frac{(k'_0 - (C_\chi)_0)(C_\chi)_0 + (k'_z - (C_\chi)_z)(C_\chi)_z}{((k'_0 - (C_\chi)_0)^2 + k'^2_\perp + (k'_z - (C_\chi)_z)^2)^2}. \quad (44)$$

After integrating the remainig variables (see the Appendix C), we find that $N = -1/(8\pi^2)$ as agreed.

B. The μ-dependent contribution

Using the result (41), we next consider the finite density contribution to Eq. (28), and compute

$$I_\rho^{\chi(2)} = i \int \frac{d^3\mathbf{k}}{(2\pi)^3} \left[\sum_{\mathrm{Re}(k_0^{\chi\#})<\mu} \mathrm{Res}\left[g_\rho^\chi(k_0,\mathbf{k})\right] \right]. \quad (45)$$

The calculation of the poles and residues is summarized in the Appendix D. The poles for the band s are located at

$$k_{0s}^{\chi\#} = -k_j(m_\chi)^j{}_0 + (C_\chi)_0 + s|\mathbf{k}' - \mathbf{C}_\chi|, \qquad s = \pm 1,$$
$$k_j' = k_i(m_\chi)^i{}_j. \quad (46)$$

It is a simple matter to verify that these poles correspond to the dispersion relations (31) of the WSM Hamiltonian (30), as expected.

The residues of $g_\rho^\chi(k_0,\mathbf{k})$ at the poles $k_{0s}^{\chi\#}$ are the real expressions

$$\mathrm{Res}[g_\rho^\chi(k_0,\mathbf{k})] = -s\frac{1}{4}\delta_\rho^j \frac{k_j' - (C_\chi)_j}{|\mathbf{k}' - \mathbf{C}_\chi|^3}. \quad (47)$$

Then we have to evaluate

$$I_\rho^{\chi(2)} = -i\delta_\rho^j \sum_{s=\pm 1} s \int \frac{d^3\mathbf{k}}{(2\pi)^3} \frac{k_j' - (C_\chi)_j}{|\mathbf{k}' - \mathbf{C}_\chi|^3} H(\mu - k_{0s}^{\chi\#})$$
$$= -i\delta_\rho^j \frac{1}{\det(m_\chi)} \sum_{s=\pm 1} s \int \frac{d^3\mathbf{k}''}{(2\pi)^3} \frac{k_j''}{|\mathbf{k}''|^3} H(\mu - k_{0s}^{\chi\#}), \quad (48)$$

where we introduce the convenient change of variables

$$k_j'' = k_j' - (C_\chi)_j, \qquad d^3\mathbf{k}'' = d^3\mathbf{k}' = \det(m_\chi)d^3\mathbf{k} \quad (49)$$

and use $\det((m_\chi)^i{}_j) = \det((m_\chi)^\mu{}_\nu) = \det(m_\chi)$, since $(m_\chi)^0{}_\nu = \delta_\nu^0$.

The next step is to calculate

$$I_j^{\chi s} = \int \frac{d^3\mathbf{k}''}{(2\pi)^3} \frac{k_j''}{|\mathbf{k}''|^3} H(\mu - k_{0s}^\#). \quad (50)$$

Recalling Eq. (27), at this stage we can write the axial part of the vacuum polarization as

$$\Pi_{A,\chi}^{\mu\nu}(p) = i\chi \frac{e^2}{2} (m_\chi^{-1})^j{}_\lambda p_\kappa \epsilon^{\mu\nu\lambda\kappa} \sum_{s=\pm 1} s I_j^{\chi s}. \quad (51)$$

Let us now rewrite the poles $k_{0s}^{\chi\#}$, in terms of the new double-primed variables k'' which enter in the integral (50). Starting from (46), the sequence $k_i(m_\chi)^i{}_0 = k_j'(m_\chi^{-1})^j{}_i(m_\chi)^i{}_0 = (k_j'' + (C_\chi)_j)(m_\chi^{-1})^j{}_i(m_\chi)^i{}_0$ yields

$$k_{0s}^{\chi\#} = \mathcal{V}_\chi \cdot \mathbf{k}'' + s|\mathbf{k}''| + E_{\chi 0}, \quad (52)$$

with the additional definitions

$$\mathcal{V}_\chi^j = (m_\chi^{-1})^j{}_i(m_\chi)^i{}_0, \qquad E_{\chi 0} = \mathcal{V}_\chi \cdot \mathbf{C}_\chi + (C_\chi)_0 \quad (53)$$

A proof of consistency can be made recalling that $k_{0s}^{\chi\#}$ describe the energy bands of the WSM. In the notation of (52) we see that the nodes are located at $\mathbf{k}'' = 0$, such that the energy of each node has to be $E_{\chi 0}$, which we know it is equal to $-\chi\tilde{b}_0$. This result is recovered from the alternative expression for $E_{\chi 0}$ in Eq. (53) after the relations (39) are used.

The simplest way to calculate $I_j^{\chi s} = -(I^{\chi s})^j$ is to realize that $\mathbf{k}/|\mathbf{k}|^3 = -\nabla(1/|\mathbf{k}|)$, which calls for an integration by parts yielding a surface term plus a volume contribution involving $\delta(k_{0s}^* - \mu)$. Also it is convenient to use spherical coordinates choosing the z-axis in the direction of $\mathcal{V}_\chi$, such that

$$k_{0s}^{\chi\#} = |\mathbf{k}''|(|\mathcal{V}_\chi|\cos\theta + s) + E_{\chi 0}. \quad (54)$$

In the following we restrict ourselves to type-I WSMs where $|\mathcal{V}_\chi| < 1$, implying that the sign of the factor of $|\mathbf{k}''|$ in (54) is independent of the angle θ, i.e., we have that $(1 + s|\mathcal{V}|\cos\theta)$ is always positive. The detailed evaluation of the integral (50) is outlined in Appendix E and we only present the results here. When $|\mathcal{V}| < 1$ the surface integral vanishes and we are left with

$$\{(I^{\chi s})^j\} = \mathbf{I}^{\chi s} = \int \frac{d^3\mathbf{k}''}{(2\pi)^3} \frac{1}{|\mathbf{k}''|} \nabla H(\mu - k_{0s}^*). \quad (55)$$

The resulting delta function imposes the condition $k_{0s}^{\chi\#} = \mu$ which we write as

$$|\mathbf{k}''|(|\mathcal{V}_\chi|\cos\theta + s) = \mu + \chi\tilde{b}_0 \equiv \Lambda_\chi. \quad (56)$$

Choosing $\mathbf{W} = \mathcal{V}_\chi$ in Eq. (E8) of the Appendix E we find

$$\mathbf{I}^{\chi s} = \left(\frac{1}{2\pi^2} \frac{1}{|\mathcal{V}_\chi|^3} (s\Lambda_\chi) H(s\Lambda_\chi) \left[|\mathcal{V}_\chi| - \mathrm{arctanh}|\mathcal{V}_\chi|\right] \right) \mathcal{V}_\chi, \quad (57)$$

which demands $(s\Lambda_\chi)$ to be positive. Going back to the vacuum polarization tensor (51) we consider a given Weyl node (fixed χ) and evaluate its contribution. Let us examine the location of the chemical potential μ relative to the position of the energy of node $E_{\chi 0} = -\chi\tilde{b}_0$. When μ is above $E_{\chi 0}$ we have $\Lambda_\chi > 0$ in such a way that only the conduction band $s = 1$ contributes with

$$[s\mathbf{I}^{\chi s}]_{s=+1} = \frac{1}{2\pi^2} \frac{1}{|\mathcal{V}_\chi|^3} \Lambda_\chi \left[|\mathcal{V}_\chi| - \mathrm{arctanh}|\mathcal{V}_\chi|\right] \mathcal{V}_\chi. \quad (58)$$

When μ is below $E_{\chi 0}$ we have the opposite situation where Λ_χ is negative and only the valence band $s = -1$ contributes with

$$[s\boldsymbol{I}^{\chi s}]_{s=-1} = \frac{1}{2\pi^2}\frac{1}{|\mathcal{V}|^3}\Lambda_\chi[|\mathcal{V}_\chi| - \mathrm{arctanh}|\mathcal{V}_\chi|]\mathcal{V}_\chi. \quad (59)$$

Summarizing, when $|\mathcal{V}| < 1$ the contribution of each node to the current results proportional to the corresponding value of Λ_χ, independently of which band provides the conducting charges, since Eq. (51) requires to consider the product $s\boldsymbol{I}^{\chi s}$ in each case. In other words, $\pi^2[s\boldsymbol{I}^{\chi s}]_{s=+1} = \pi^2[s\boldsymbol{I}^{\chi s}]_{s=-1} \equiv N_\chi\mathcal{V}_\chi$ with

$$N_\chi = \frac{1}{2|\mathcal{V}|^3}\left[|\mathcal{V}_\chi| - \mathrm{arctanh}|\mathcal{V}_\chi|\right]. \quad (60)$$

The final result for Eq. (51) is

$$\Pi_{A,\chi}^{\mu\nu}(p) = i\frac{e^2}{2\pi^2}p_\kappa\epsilon^{\mu\nu\lambda\kappa}\sum_{\chi=\pm1}\chi\Lambda_\chi N_\chi(m_\chi^{-1})^j_{\ \lambda}(\mathcal{V}_\chi)_j, \quad (61)$$

from where we read

$$\mathcal{B}_\lambda^{(2)} = -\sum_{\chi=\pm1}\chi\Lambda_\chi N_\chi(m_\chi^{-1})^j_{\ \lambda}(\mathcal{V}_\chi)_j, \quad (62)$$

according to (14). In the Appendix F we put together the separate contributions to $\mathcal{B}_\lambda$ in Eqs. (43) and (62), expressing the final result in terms of the parameters of the WSM Hamiltonian (30). We obtain

$$\mathcal{B}_0 = \tilde{b}_0 - \sum_{\chi=\pm1}\chi\Lambda_\chi N_\chi v_\chi^i\left[(\mathbb{A}_\chi^{-1})^T(\mathbb{A}_\chi^{-1})\right]_{ij}v_\chi^j, \quad (63)$$

$$\mathcal{B}_k = \tilde{b}_k + \sum_{\chi=\pm1}\chi\Lambda_\chi N_\chi\left[(\mathbb{A}_\chi^{-1})^T(\mathbb{A}_\chi^{-1})\right]_{kl}v_\chi^l, \quad (64)$$

with

$$\begin{aligned}&\Lambda_\chi = \mu + \chi\tilde{b}_0, \qquad (\mathcal{V}_\chi)^i = (\mathbb{A}_\chi^{-1})_{ik}v_\chi^k,\\&N_\chi = \frac{1}{2|\mathcal{V}_\chi|^3}(|\mathcal{V}_\chi| - \mathrm{arctanh}(|\mathcal{V}_\chi|)),\\&|\mathcal{V}_\chi| = \sqrt{(\mathcal{V}_\chi)^i(\mathcal{V}_\chi)^i}.\end{aligned} \quad (65)$$

V. A CHIRAL KINETIC THEORY APPROACH

We now validate our results by using chiral kinetic theory, which is a topologically modified semiclassical Boltzmann formalism to describe the behavior of Weyl fermions at finite chemical potential. In the presence of an electric field, in addition to the usual band dispersion, the velocity for Bloch electrons acquires an extra term proportional to the Berry curvature [95,96]. This gives rise to a transverse topological current given by

$$\mathbf{J} = -\frac{e^2}{\hbar}\sum_s\sum_{\chi=\pm1}\int\frac{d^3\mathbf{k}}{(2\pi)^3}\mathbf{E}\times\mathbf{\Omega}_{s\chi}(\mathbf{k})f_{s\chi}^{\mathrm{F.D.}}(\mathbf{k}), \quad (66)$$

where $\mathbf{E}$ denotes the electric field, $f_{s\chi}^{\mathrm{F.D.}}(\mathbf{k})$ is the Fermi-Dirac distribution function for Bloch electrons with chirality χ in the s-th band and $\mathbf{\Omega}_{s\chi}(\mathbf{k}) = i\langle\nabla_{\mathbf{k}}u_{s\chi}(\mathbf{k})| \times |\nabla_{\mathbf{k}}u_{s\chi}(\mathbf{k})\rangle$ is the Berry curvature. Here, the Bloch states $|u_{s\chi}(\mathbf{k})\rangle$ are defined by $\hat{H}_\chi|u_{s\chi}(\mathbf{k})\rangle = E_{s\chi}|u_{s\chi}(\mathbf{k})\rangle$, where $\hat{H}_\chi$ is the single particle Hamiltonian for a Weyl fermion with chirality χ. Evaluation of the Hall current from Eq. (66) reproduces the Karplus-Luttinger formula for the anomalous Hall conductivity [97]. In the following we evaluate the anomalous Hall current (66) for a WSM described by the model Hamiltonian (30) characterized by the tilting v_χ and the matrix of the Fermi velocities $\mathbb{A}_\chi$, which we consider symmetric in this section.

The topological properties of the two-node model $H_\chi(\mathbf{k})$ under consideration can be seen from the Berry curvature. Using the Bloch states $|u_{s\chi}(\mathbf{k})\rangle$ the Berry curvature is found to be

$$\mathbf{\Omega}_{s\chi}(\mathbf{k}) = -\frac{s\chi}{2}\det(\mathbb{A}_\chi)\frac{\mathbb{A}_\chi^{-1}\mathcal{K}_\chi}{\mathcal{K}_\chi^3}. \quad (67)$$

In the isotropic limit this expression reduces to the usual monopole-like Berry curvature of the Weyl nodes. Furthermore, we can check that the Berry flux piercing any surface enclosing the node is exactly $2\pi\chi$. From Eq. (67) we compute the topological current. First, we rewrite Eq. (66) in the standard form of the anomalous Hall current $\mathbf{J} = \frac{e^2}{2\pi^2}\delta\mathcal{B}\times\mathbf{E}$, where

$$\delta\mathcal{B} = 2\pi^2\sum_s\sum_{\chi=\pm1}\int\frac{d^3\mathbf{k}}{(2\pi)^3}\mathbf{\Omega}_{s\chi}(\mathbf{k})f_{s\chi}^{\mathrm{F.D.}}(\mathbf{k}). \quad (68)$$

Here we have introduced $\delta\mathcal{B}$ instead of the full $\mathcal{B}$ of the previous section because the semiclassical approximation fails to predict the Hall current proportional to the Weyl node separation. This is expected because the semiclassical approximation accounts for the single-band Fermi surface properties of the wave packets, and the Hall conductivity carries information of all filled states. To evaluate the integral (68) we change the integration variable from $\mathbf{k}$ to $\mathcal{K}_\chi$. Substituting the Berry curvature (67), the expression (68) in the zero-temperature limit becomes

$$\begin{aligned}\delta\mathcal{B} = -\pi^2\sum_s\sum_{\chi=\pm1}s\chi\mathbb{A}_\chi^{-1}\int\frac{d^3\mathcal{K}_\chi}{(2\pi)^3}\frac{\mathcal{K}_\chi}{\mathcal{K}_\chi^3}\\\times H(\mu + \chi\tilde{b}_0 - \mathcal{V}_\chi\cdot\mathcal{K}_\chi - s\mathcal{K}_\chi).\end{aligned} \quad (69)$$

This integral is exactly the same obtained when evaluating the μ-dependent contribution to the vacuum polarization

tensor in Sec. IV B. See Eq. (50) for instance. A detailed solution of this integral is presented in the Appendix E and here we take the final result only.

For a type-I WSM, defined by $\mathcal{V}_\chi = |\mathcal{V}_\chi| < 1$, the μ-dependent correction to the anomalous Hall current is expressed in terms of the vector

$$\delta\boldsymbol{\mathcal{B}} = -\sum_{\chi=\pm1} \frac{\chi\Lambda_\chi}{2\mathcal{V}_\chi^3} \left[\mathcal{V}_\chi - \operatorname{arctanh}(\mathcal{V}_\chi) \right] \mathbb{A}_\chi^{-1} \mathbb{A}_\chi^{-1} \boldsymbol{v}_\chi, \quad (70)$$

where $\Lambda_\chi = \mu + \chi\tilde{b}_0$. This result reproduces the one obtained in the previous section, where it was derived within a quantum field theoretical approach, since $\delta\boldsymbol{\mathcal{B}}$ is equal to $\boldsymbol{\mathcal{B}}^{(2)}$ defined in the previous section.

VI. APPLICATIONS

In Weyl semimetals the energy spectrum around band-touching points behaves as tilted and anisotropic Dirac cones. These differences from the ideal Dirac cone picture, where the charge carriers behave as massless relativistic particles, have important consequences for the physical properties of Weyl semimetals as well as for their optical and transport features.

In recent years, there has been a great deal of interest in measuring transport properties induced by the Berry curvature, specially the anomalous Hall effect [98]. In experiments, there are a number of factors which make difficult the measurement of the ideal anomalous Hall effect $\mathbf{J} = \frac{e^2}{2\pi^2}\tilde{\boldsymbol{b}} \times \mathbf{E}$. For example, since the Weyl nodes do not lie exactly at the Fermi level, other factors are expected to be relevant, such as the anisotropy, tilting and disorder. However, as shown in Ref. [99], disorder-induced contributions to the anomalous Hall conductivity are absent when the Fermi level is near the nodes, thus leaving the anisotropy and tilting as possible responsible of deviations from the ideal prediction. In this section we aim to fill in this gap. Here, we use the theory developed in the previous sections to investigate the anomalous Hall current for different WSM materials, mainly focusing on the effects of the tilting and the anisotropy.

A. The ideal Weyl semimetal EuCd$_2$As$_2$

The simple structure of Weyl nodes in the trigonal crystal EuCd$_2$As$_2$ makes it an ideal material with which to study the different contributions to the anomalous Hall effect. *Ab initio* electronic structure calculations reveal that EuCd$_2$As$_2$ has only a single pair of Weyl nodes located at $\pm\tilde{\boldsymbol{b}} = (0,0,\pm\tilde{b}_z)$ along the c axis, with $\tilde{b}_z = 0.03 \times 2\pi/c \approx 0.26$ nm^{-1}. Inversion symmetry guarantees that the nodes lie at the same energy, i.e., $\tilde{b}_0 = 0$. If the nodes lie at the Fermi level, *ab initio* calculations predict the anomalous Hall conductivity to be $\sigma_{yx}^{\text{AHC}} = \frac{e^2\tilde{b}_z}{2\pi^2\hbar} \approx 30\Omega^{-1}$ cm^{-1}, which is significantly larger than the observed value which is of

the order of $0.5\Omega^{-1}$ cm^{-1} [100]. This prediction is valid when the nodes lie at the Fermi level, however, in the experiments carried out by authors in Ref. [100], the nodes are slightly shifted from the Fermi level. In this case, as our results in Eqs. (64) and (70) anticipate, the anisotropy and tilting contribute to the anomalous Hall conductivity by replacing $\tilde{\boldsymbol{b}}$ to $\tilde{\boldsymbol{b}} + \delta\boldsymbol{\mathcal{B}}$. In the following we estimate such corrections. To this end, we use the low-energy linearly-dispersing two-band model derived in Ref. [100]. The effective Hamiltonian for a Weyl node of chirality χ is given by Eq. (30), with $\boldsymbol{v}_\chi = (0,0,\chi v)$ and $\mathbb{A}_\chi = \chi\operatorname{diag}(v_\parallel, v_\parallel, \chi v_\perp)$. These velocity parameters are obtained by fitting the energy computed from *ab initio* calculations. The obtained values are $v = 1.6v_0$, $v_\parallel = 3v_0$ and $v_\perp = 2v_0$, where $v_0 = 1.51 \times 10^5$ m/s. Furthermore, from Shubnikov–de Haas measurements and *ab initio* calculations, the Fermi level is predicted to be approximately 52 meV below the Weyl nodes thus lying in the valence band. All in all, the shift of the Weyl node position (70) is found to be $\delta\boldsymbol{\mathcal{B}} = (0,0,-0.122)$ nm^{-1}, such that the anomalous Hall conductivity becomes

$$\tilde{\sigma}_{yx}^{\text{AHC}} = \frac{e^2(\tilde{b}_z + \delta\mathcal{B}_z)}{4\pi^2\hbar} \approx 15.9\Omega^{-1} \text{ cm}^{-1}, \quad (71)$$

which represents a significant reduction from the originally predicted anomalous Hall conductivity σ_{yx}^{AHC}. However there are other factors which could diminish further the conductivity, for example, finite temperature effects and higher-order terms in the model Hamiltonian.

B. The highly anisotropic and tilted monopnictide TaAs

We will now apply our results to the archetypal nonmagnetic transition-metal monopnictide TaAs, the best-known WSM [71]. This material crystallizes in a body-centered tetragonal structure with lattice parameters $a = b = 0.34348$ nm^{-1} and $c = 1.1641$ nm^{-1}. In the Brillouin zone of TaAs, there are 24 Weyl nodes in total; 8 Weyl nodes on the $k_z = 2\pi/c$ plane (W1 nodes) and 16 Weyl nodes away from the $k_z = 2\pi/c$ plane (W2 nodes). W1 (W2) nodes are located 26 meV (13 meV) below the Fermi level, which crosses only the conduction band (electron pockets). The electronic structure of TaAs shows that the Weyl bands around the W1 and W2 nodes possess strong anisotropies and tilting. Since the Weyl nodes are separated in the k_x-direction, a linear fit of the Weyl bands near the nodes produces an effective Hamiltonian as given by Eq. (30), such that the tilting and matrix of Fermi velocities depend if the node is either W1 or W2. Extracted from *ab initio* calculations of Ref. [101], for W1 nodes the band parameters are

$$\mathbb{A}_\chi^{\text{W1}} = \chi v_0' \begin{pmatrix} 3.963\chi & 0.393\chi & 0 \\ 0.393\chi & 2.318 & 0 \\ 0 & 0 & 0.212 \end{pmatrix},$$

$$\nu_\chi^{\text{W1}} = v_0' \begin{pmatrix} -1.603\chi \\ 1.004 \\ 0 \end{pmatrix}, \tag{72}$$

and for the W2 nodes we have

$$\mathbb{A}_\chi^{\text{W2}} = \chi v_0' \begin{pmatrix} 3.220\chi & 1.127\chi & 0.661\chi \\ 1.127\chi & 0.291 & 2.464 \\ 0.661\chi & 2.464 & 1.659 \end{pmatrix},$$

$$\nu_\chi^{\text{W2}} = v_0' \begin{pmatrix} -0.989\chi \\ 0.944 \\ 1.409 \end{pmatrix}, \tag{73}$$

where $v_0' = 1 \times 10^5$ m/s. These parameter values support the picture of highly anisotropic and strongly tilted Weyl cones in TaAs. Besides, note that W1 Weyl bands are almost 2D, while W2 bands are 3D. With all the information above, we are able to compute the correction to the anomalous Hall conductivity by using our equivalent formulas (62) and (70). The contributions to the shifting from the W1 and W2 nodes are found to be

$$\delta\mathcal{B}^{\text{W1}} = \begin{pmatrix} 0.01719 \\ -0.00655 \\ 0 \end{pmatrix} \text{nm}^{-1},$$

$$\delta\mathcal{B}^{\text{W2}} = \begin{pmatrix} -0.04814 \\ 0.02670 \\ 0.01967 \end{pmatrix} \text{nm}^{-1}, \tag{74}$$

respectively. Here, we used that $\Lambda_\chi^{\text{W1}} = 26$ meV and $\Lambda_\chi^{\text{W2}} = 13$ meV, which are the positions of the W1 and W2 nodes below the Fermi level. We observe that the shifting of the W1 nodes are confined to the x–y plane, consistent with the fact that Weyl bands are almost 2D. The full contribution to the anomalous Hall conductivity can be obtained by summing up the contributions from the 12 pairs of nodes of TaAs, i.e.,

$$\delta\mathcal{B} = \sum_{i=1,2} N_i \delta\mathcal{B}^{\text{W}i} = \begin{pmatrix} -0.31639 \\ 0.18741 \\ 0.15743 \end{pmatrix} \text{nm}^{-1}, \tag{75}$$

where we used $N_1 = 4$ and $N_2 = 8$, which are the number of pairs of $W1$ and $W2$ nodes in the Brillouin zone of TaAs. Interesting conclusions can be extracted from this result. First, we observe that the effects of the anisotropy and

tilting can be clearly distinguished from the conventional anomalous Hall current, which is proportional to the Weyl nodes separation. In the present case the nodes are separated along the x axis and hence the anomalous Hall conductivity is $\sigma_{zy}^{\text{AHC}} = \frac{e^2 \tilde{b}_x}{2\pi^2 \hbar}$. However, in the presence of anisotropy and tilting, the resulting anomalous Hall current is

$$\tilde{\sigma}_{zy}^{\text{AHC}} = \frac{e^2(\tilde{b}_x + \delta\mathcal{B}_x)}{2\pi^2\hbar}, \qquad \tilde{\sigma}_{yx}^{\text{AHC}} = \frac{e^2\delta\mathcal{B}_z}{2\pi^2\hbar},$$

$$\tilde{\sigma}_{xz}^{\text{AHC}} = \frac{e^2\delta\mathcal{B}_y}{2\pi^2\hbar}. \tag{76}$$

Therefore, the two last terms are purely induced by anisotropy and tilting.

Finally, it is worth mentioning that our analysis can also be applied to other WSM materials of the TaAs family, such as TaP, NbAs, and NbP. These materials are also highly anisotropic and tilted, however, unlike TaAs where only electrons pockets occurs, *ab initio* calculations indicate that in these other WSMs both electron pockets for W1 nodes and hole pockets for W2 nodes occur [101].

VII. SUMMARY AND RESULTS

In quantum field theory the calculation of the effective action $S_{\text{eff}}(A^\mu)$ starting from a fermionic system minimally coupled to external electromagnetic fields A^μ provides a very general method to obtain the effective current $J_\mu^{\text{eff}}(x) = \delta S_{\text{eff}}/\delta A^\mu(x)$ yielding the response of the system. For a wide class of materials this procedure gives an alternative to some strategies frequently used in condensed matter physics to determine the electromagnetic response of a medium, such as to the Kubo linear response theory and the chiral kinetic theory approach, for example. Such particular set of materials include fermionic excitations having a dispersion relation which is linear near the band-touching points in the Brillouin zone close to the Fermi energy, thus signaling the presence of Dirac-Weyl quasiparticles akin to the real particles resulting in the fundamental interactions of high-energy physics. Nevertheless, a fundamental difference arises since the periodic and bounded structure of a crystaline lattice induce the violation of the spacetime symmetries such as translations, continuous rotations and Lorentz invariance. Fortunately, a quantum field theory model has been constructed to deal with such violations; the SME. Its minimal fermionic sector covers many Dirac-Weyl Hamiltonians coinciding with the linearized version, near the Fermi energy, of the tight-binding Hamiltonians describing materials such as topological insulators and Dirac-Weyl semimetals, for example.

Having in mind the application of our results to the realistic case of a Weyl semimetal with tilting and anisotropy we considered the selection (4) of parameters in the SME, which embodies those included in the condensed

matter Hamiltonian (30). The resulting fermionic action is chiral, which simplifies enormously the calculation of the *CPT*-odd contribution of the vacuum polarization tensor $\Pi_A^{\mu\nu}$ that can be further split into the sum of the two chiral contributions. This tensor determines the *CPT*-odd effective action in our approximation of two powers in the external electromagnetic field. We restrict ourselves to this sector since it produces novel effects such as the anomalous Hall current and a contribution to the chiral magnetic effect. Our calculation is nonperturbative in the parameters of the model and yields the general result that the ensuing effective electrodynamics remains of the axionic type (2) with $\Theta(x) = \mathcal{B}_\mu x^\mu$, where $\mathcal{B}_\mu$ is the main objective of the calculation being related to $\Pi_A^{\mu\nu}$ through Eq. (14). The results, previous to the inclusion of finite density effects are given in Eq. (29) for each chirality. They are presented in terms of the chosen LIV parameters of the SME, but can also be expressed using those of the condensed matter Hamiltonian employing Eq. (39).

The filling of the valence and the conduction bands with respect to the Fermi energy determines the conduction properties of the material and we introduce this dependence through the chemical potential μ. This naturally split the basic integral (29) into a μ-independent piece plus a μ-dependent one. In the first contribution we face the well-known and much discussed problem that the overall factor of the integral is finite but undetermined. We fix this ambiguity by selecting the factor $N = -1/(8\pi)^2$ that reproduces the anomalous Hall conductivity $\sigma_{xy} = -e^2 \tilde{b}_z/(2\pi)^2$ in the isotropic case with no tilting and when the cones are separated along the z-axis. After we rely on the residual rotational symmetry in the presence of the vector **C** to perform a first integration, we show that this factor is obtained when we introduce a cutoff along the direction where each of the remaining integrals diverge. To deal with the second μ-dependent contribution we extend the integral (28) to the imaginary time using the Matsubara formalism at zero temperature and calculate it following the prescription (41). This yields our final result for the vector $\mathcal{B}_\lambda$ presented in Eqs. (63)–(65) in terms of the parameters of the condensed matter Hamiltonian.

We have also obtained the anomalous Hall current from the chiral kinetic theory approach. In this case, within the linear approximation we are considering, the predicted value for the μ-independent part is zero. Assuming a symmetric anisotropy matrix we get the result in (70) for the μ-dependent contribution, which coincides with that in Eq. (64) calculated via the effective action. The contribution from $\mathcal{B}_0$ can also be obtained within the semiclassical approach. This agreement, together with the result itself, constitutes the most important conclusion of our work showing the strength of effective action calculations in WSMs.

Our final results are further limited to type-I WSMs, where the magnitude of the effective tilting parameter V_χ is less than one. In this case the integral $\mathbf{I}^{\chi s}$, common to both methods and calculated in the Appendix E, has no singularities in the angular range of integration. Different from type-I WSMs, the energy values of Weyl nodes in type-II WSM are not the local extrema. Their discussion would require introducing additional cutoffs in the model, which may be material dependent, so we consider this situation beyond the scope of the present work. In our case the contribution to the conductivity of each node is due to a single band s which is determined by the sign of $\Lambda_\chi = \mu - E_0$ according to the condition $s\Lambda_\chi > 0$. The constant Λ_χ measures the location of the chemical potential with respect to the energy of the node E_0.

We include two applications that show the important consequences of the tilted and anisotropic Dirac cones for the transport properties of Weyl semimetals, focusing upon the anomalous Hall current.

In the first case of the ideal Weyl semimetal $EuCd_2As_2$, described in Sec. VI A, we find that the contribution $\delta\mathcal{B}$, resulting with components only in the direction of the separation $\tilde{\mathbf{b}}$ of the nodes, lowers down the *ab initio* calculations of the anomalous Hall conductivity $\sigma_{yx}^{\text{AHC}} \approx 30\,\Omega^{-1}\,\text{cm}^{-1}$ to the value $\sigma_{yx}^{\text{AHC}} \approx 15.9\,\Omega^{-1}\,\text{cm}^{-1}$ which is much closer to the measured value of $0.5\,\Omega^{-1}\,\text{cm}^{-1}$. However there are other factors which could diminish further the conductivity such as finite temperature effects and higher-order terms in the model Hamiltonian, which are not considered in our calculations.

The second application in Sec. VI B concerns TaAs, the best known WSM. Here we have the proliferation of 24 Weyl nodes, split in two families, 8 of them denoted by W1 located on the $k_z = 2\pi/c$ plane, together with the remaining 16 W2 nodes placed away from this plane. The separation of each pair of nodes is along the k_x direction such that only the ideal anomalous Hall conductivity σ_{zy}^{AHC} should be nonzero. Nevertheless, tilting and anisotropy endow the correction $\delta\mathcal{B}$ with components along the three directions yielding nonzero contributions to σ_{yx}^{AHC} and σ_{xz}^{AHC}, clearly distinguished from the conventional anomalous Hall conductivity, and which could in principle be measured. Finally, it is worth mentioning that our analysis can be extended to other WSM materials of the TaAs family, such as TaP, NbAs, and NbP, which are also highly anisotropic and tilted, which nevertheless present additional challenges not fully covered in this work.

APPENDIX A: THE PROJECTION OF THE PROPAGATORS

To evaluate the trace appearing in Eq. (23) for the vacuum polarization tensor we have to know the action of the projection operator P_χ to the right of the propagator $S(k)$. In the case of a massless standard fermion this is a simple task, since the propagator $i/k_\mu \gamma^\mu$ can be readily rationalized as $ik_\mu \gamma^\mu/k^2$. However in the problem at hand, the presence of the γ^5 is the denominator of the propagator requires a more subtle analysis, since the projectors do not have an inverse which could be directly applied to the denominator. To tackle this problem in a general frame, we introduce two numerical vectors U_μ and V_μ, and define $(\slashed{U} - \gamma^5 \slashed{V})^{-1}$, with the usual slash notation $\slashed{U} = U_\mu \gamma^\mu$. Assuming that $\slashed{U}$ has a inverse given by $\slashed{U}^{-1} = \slashed{U}/U^2$, with $U^2 = U_\mu U^\mu$, we consider the following sequence:

$$\frac{1}{\slashed{U} - \gamma^5 \slashed{V}} = \frac{1}{1 - \frac{\slashed{U}}{U^2}\gamma^5\slashed{V}}\frac{\slashed{U}}{U^2} = \sum_n \left(\frac{\slashed{U}}{U^2}\gamma^5\slashed{V}\right)^n \frac{\slashed{U}}{U^2}$$

$$= \frac{\slashed{U}}{U^2} \sum_n \left(\frac{1}{U^2}\gamma^5\slashed{V}\slashed{U}\right)^n. \quad (A1)$$

Now, we have to apply this expression to the projector P_χ. To this end we use the identities $\gamma^\mu P_\chi = P_{-\chi}\gamma^\mu$ and $\gamma^5\gamma^\mu P_\chi = -\gamma^\mu\gamma^5 P_\chi = -\chi\gamma^\mu P_\chi$, such that

$$\gamma^5\slashed{V}\slashed{U}P_\chi = \gamma^5 V_\mu \gamma^\mu U_\nu \gamma^\nu P_\chi = \gamma^5 V_\mu \gamma^\mu P_{-\chi} U_\nu \gamma^\nu$$

$$= \chi V_\mu \gamma^\mu U_\nu \gamma^\nu = \chi P_\chi \slashed{V}\slashed{U}. \quad (A2)$$

In this way, using the relation (A2) for each motion of the projector P_χ to the left of a product $\slashed{V}\slashed{U}$ we obtain

$$\frac{1}{\slashed{U} - \gamma^5 \slashed{V}}P_\chi = \frac{\slashed{U}}{U^2}\sum_n \left(\frac{1}{U^2}\gamma^5\slashed{V}\slashed{U}\right)^n P_\chi$$

$$= \frac{\slashed{U}}{U^2}P_\chi\sum_n \left(\frac{1}{U^2}\chi\slashed{V}\slashed{U}\right)^n$$

$$= P_{-\chi}\sum_n \frac{\slashed{U}}{U^2} \left(\frac{1}{U^2}\chi\slashed{V}\slashed{U}\right)^n, \quad (A3)$$

where from we read the identity

$$\frac{1}{\slashed{U} - \gamma^5 \slashed{V}}P_\chi = P_{-\chi}\frac{1}{\slashed{U} - \chi\slashed{V}}. \quad (A4)$$

With the help of this result we can now evaluate the quantity $S(k)\gamma^\mu P_\chi$, where $S(k) = i(\Gamma^\mu k_\mu - M)^{-1}$ is the fermion propagator with $\Gamma^\mu = \gamma^\mu + c^\mu{}_\nu\gamma^\nu + d^\mu{}_\nu\gamma^5\gamma^\nu$ and $M = a_\mu\gamma^\mu + b_\mu\gamma^5\gamma^\mu$. In this way

$$S(k)\gamma^\nu P_\chi = \frac{i}{\Gamma^\mu k_\mu - M}P_{-\chi}\gamma^\nu \equiv P_\chi S_\chi(k)\gamma^\nu, \quad (A5)$$

where

$$S_\chi(k) = \frac{i}{[k_\mu(m_\chi)^\mu{}_\nu - (C_\chi)_\nu]\gamma^\nu} \quad (A6)$$

is interpreted as the propagator for a fermion of chirality χ with

$$(m_\chi)^\mu{}_\nu = \delta^\mu{}_\nu + c^\mu{}_\nu - \chi d^\mu{}_\nu, \qquad (C_\chi)_\nu = a_\nu - \chi b_\nu. \quad (A7)$$

APPENDIX B: CALCULATION OF THE POLARIZATION TENSOR

The goal of this section is to evaluate the vacuum polarization of a fermion with chirality χ, as defined by Eq. (26). Substituting the chiral propagator (A6) into Eq. (26) one gets

$$i\Pi_\chi^{\mu\nu}(p) = e^2 (m_\chi)^\mu{}_\beta (m_\chi)^\nu{}_\alpha \int \frac{d^4k}{(2\pi)^4} \text{tr}$$

$$\times \left\{ \frac{i}{[(k_\lambda - p_\lambda)(m_\chi)^\lambda{}_\tau - (C_\chi)_\tau]\gamma^\tau} \right.$$

$$\left. \times \gamma^\beta \frac{i}{[k_\sigma m^\sigma{}_\xi - (C_\chi)_\xi]\gamma^\xi}\gamma^\alpha P_\chi \right\}. \quad (B1)$$

Since our main concern in this paper is to calculate the *CPT*-odd contribution to the effective action of a general WSM, we now retain only the axial part of the vacuum polarization tensor, which arises from selecting the $\chi\gamma^5/2$ part of the projector in the right of Eq. (B1). To simplify further such expression, we introduce the change of variables $k'_\nu = k_\mu(m_\chi)^\mu{}_\nu$ such that $d^4k = \frac{1}{\det m_\chi}d^4k'$ and define $p'_\nu = p_\mu(m_\chi)^\mu{}_\nu$. For simplicity in the notation we do not explicitly write the χ-dependence of the primed variables k'_ν and p'_ν. All in all, Eq. (B1) becomes

$$i\Pi_\chi^{\mu\nu}(p) = \frac{\chi}{2}e^2 (m_\chi)^\mu{}_\beta (m_\chi)^\nu{}_\alpha \frac{1}{\det m_\chi}\int \frac{d^4k'}{(2\pi)^4}\text{tr}$$

$$\times \left[\frac{i}{(k' - p' - C_\chi)_\tau\gamma^\tau}\gamma^\beta \frac{i}{(k' - C_\chi)_\xi\gamma^\xi}\gamma^\alpha\gamma^5 \right]. \quad (B2)$$

Rationalizing the propagators and taking the trace using $\text{tr}(\gamma^\tau\gamma^\beta\gamma^\xi\gamma^\alpha\gamma^5) = -4i\epsilon^{\tau\beta\xi\alpha}$ with $\epsilon^{0123} = +1$ we get

$$i\Pi_\chi^{\mu\nu}(p) = -\frac{\chi}{2}e^2(m_\chi)^\mu{}_\beta(m_\chi)^\nu{}_\alpha \frac{1}{\det m_\chi}\int \frac{d^4 k'}{(2\pi)^4}\text{tr}$$

$$\times \left[\frac{(k' - p' - C_\chi)_\tau}{(k' - p' - C_\chi)^2}\frac{(k' - C_\chi)_\xi}{(k' - C_\chi)^2}\gamma^\tau\gamma^\beta\gamma^\xi\gamma^\alpha\gamma^5\right]$$

$$= -2\chi e^2(m_\chi)^\mu{}_\beta(m_\chi)^\nu{}_\alpha \frac{1}{\det m_\chi}\epsilon^{\tau\beta\xi\alpha}$$

$$\times \int \frac{d^4 k'}{(2\pi)^4}\frac{p'_\tau(k' - C_\chi)_\xi}{(k' - p' - C_\chi)^2(k' - C_\chi)^2}, \qquad \text{(B3)}$$

which is the exact nonperturbative result. Since we are looking for the contribution to Eq. (14) with only one power of the external momenta, we set $p' = 0$ in the denominator. A further simplification arises due to the identity,

$$m^\mu{}_\alpha m^\nu{}_\beta \epsilon^{\alpha\beta\rho\sigma}p'_\rho = p_\kappa(\det m_\chi)(m_\chi^{-1})^\sigma{}_\lambda \epsilon^{\mu\nu\lambda\kappa}, \quad \text{(B4)}$$

yielding our final result of Eq. (27), with the function $I_\rho^\chi(C)$ defined by Eq. (28).

APPENDIX C: THE μ-INDEPENDENT CONTRIBUTION

We now explicitly compute the integral (44)

$$N = \frac{1}{C_\chi^2(2\pi)^4}\int_{-\infty}^\infty dk'_0 \int_{-\infty}^\infty dk'_z \int_0^{2\pi} d\phi \int_0^\infty dk'_\perp k'_\perp$$

$$\times \frac{(k'_0 - (C_\chi)_0)(C_\chi)_0 + (k'_z - (C_\chi)_z)(C_\chi)_z}{((k'_0 - (C_\chi)_0)^2 + k_\perp'^2 + (k'_z - (C_\chi)_z)^2)^2}.$$

Here the integrals over ϕ and $k'_\perp$ are finite and can be immediately calculated. Therefore, after integrating, we obtain

$$N_\chi = \frac{1}{2C_\chi^2(2\pi)^3}(I_0 + I_z), \qquad \text{(C1)}$$

where

$$I_0 = (C_\chi)_0 \int_{-\infty}^\infty dk'_0 \int_{-\infty}^\infty dk'_z \frac{(k'_0 - (C_\chi)_0)}{(k'_0 - (C_\chi)_0)^2 + (k'_z - (C_\chi)_z)^2}, \qquad \text{(C2)}$$

and

$$I_z = (C_\chi)_z \int_{-\infty}^\infty dk'_0 \int_{-\infty}^\infty dk'_z \frac{(k'_z - (C_\chi)_z)}{(k'_0 - (C_\chi)_0)^2 + (k'_z - (C_\chi)_z)^2}. \qquad \text{(C3)}$$

For I_0 the integral over k'_z is finite, whereas the integral over k_0 shows a logarithmic divergence. Consequently, a cut-off

is introduced in the k'_0 direction. To compute this integral, we initiate the process by integrating over k'_z through the introduction of the substitution

$$(k'_z - (C_\chi)_z)^2 \to (k'_0 - (C_\chi)_0)^2 \tan^2\theta \Rightarrow dk'_z$$
$$= |k'_0 - (C_\chi)_0|\sec^2\theta d\theta. \qquad \text{(C4)}$$

Then, integrating over θ, we arrive at

$$I_0 = \pi(C_\chi)_0 \int_{-\Lambda_0}^{\Lambda_0} dk'_0 \text{sgn}(k'_0 - (C_\chi)_0)$$

$$= \pi(C_\chi)_0 \left(\int_{-\Lambda_0}^{(C_\chi)_0} dk'_0 \text{sgn}(k'_0 - (C_\chi)_0)\right.$$

$$\left. + \int_{(C_\chi)_0}^{\Lambda_0} dk'_0 \text{sgn}(k'_0 - (C_\chi)_0)\right)$$

$$= \pi(C_\chi)_0\left[-((C_\chi)_0 + \Lambda_0) + \Lambda_0 - (C_\chi)_0\right]$$

$$= -2\pi(C_\chi)_0^2. \qquad \text{(C5)}$$

This yields a finite result in which the divergences disappear. For I_z, the situation is equivalent, with the difference that, in this case, the integral over k'_0 is finite while the integral over k'_z displays a logarithmic divergence. Proceeding in analogous way to the previous case, we find that

$$I_z = -2\pi(C_\chi)_z^2. \qquad \text{(C6)}$$

So, finally, we obtain

$$N = -\frac{1}{8\pi^2}. \qquad \text{(C7)}$$

APPENDIX D: CALCULATION OF THE POLES AND RESIDUES OF $g_\rho^\chi(k_0,\boldsymbol{k})$

To evaluate the μ-dependent contribution to the vacuum polarization tensor we have to calculate the integral (45), which requires first to determine the poles in the variable k_0 of the function $g_\rho^\chi(k_0,\boldsymbol{k})$ defined by Eq. (28), together with the corresponding residues.

1. The poles

Let us start by finding the positions $k_{0s}^{\chi\#}$ of the double poles of $g_\rho^\chi(k_0,\boldsymbol{k})$ in the k_0-plane. From Eq. (28) we see that they are located (in primed coordinates) at the two points $k'_{0s} = (C_\chi)_0 + s|\boldsymbol{k}' - \boldsymbol{C}_\chi|$. To find the corresponding $k_{0s}^{\chi\#}$ we recall the relations $k'_0 = k_\mu(m_\chi)^\mu{}_0$ and $k'_i = k_0(m_\chi)^0{}_i + k_j(m_\chi)^j{}_i$, together with our general condition $(m_\chi)^0{}_\nu = \delta^0{}_\nu$ arising from the linearized Hamiltonian (30). Under this assumption, which avoids the mixing of k_0 and k_i in k'_j, the poles are located at

$$k_{0s}^{\chi\#} = -k_j(m_\chi)^j{}_0 + (C_\chi)_0 + s|\boldsymbol{k}' - \boldsymbol{C}_\chi|, \qquad \text{(D1)}$$

where $s = \pm 1$ denotes the band index. Using the equivalences in Eq. (39), one can further verify that the resulting poles in the energy variable correspond exactly to the values of the energy obtained from the dispersion relation (31) calculated from the model Hamiltonian (30). To see this, let us start from Eq. (39) where we read that $(m_\chi)^i{}_0 = v^i_\chi$, $(m_\chi)^i{}_j = (A_\chi)_{ij}$, $(C_\chi)_0 = \chi(v^i_\chi \tilde{b}^i - \tilde{b}_0)$ and $(C_\chi)_j = \chi\tilde{b}^i(A_\chi)_{ij}$. The substitution of these relations into the right hand side of Eq. (D1) yields $k_{0s}^{\chi\#} = E_{s\chi}(\boldsymbol{k})$.

For later use in the main text we introduce double-primed momenta defined by the shifting $\boldsymbol{k}'' = \boldsymbol{k}' - \boldsymbol{C}_\chi$, such that the poles (D1) can be written in the simple form,

$$k_{0s}^{\chi\#} = \boldsymbol{\mathcal{V}}_\chi \cdot \boldsymbol{k}'' + s|\boldsymbol{k}''| + E_{\chi 0}, \qquad \text{(D2)}$$

where we define $\mathcal{V}^j_\chi = (m_\chi^{-1})^j{}_i(m_\chi)^i{}_0$ and $E_{\chi 0} = \boldsymbol{\mathcal{V}}_\chi \cdot \boldsymbol{C}_\chi + (C_\chi)_0$. To derive this result we use the sequence of relations: $k_i(m_\chi)^i{}_0 = k'_j(m_\chi^{-1})^j{}_i(m_\chi)^i{}_0 = [k''_j + (C_\chi)_j](m_\chi^{-1})^j{}_i(m_\chi)^i{}_0$. In the double-primed coordinates the gap closing condition

(defining the nodes) is $\boldsymbol{k}'' = \boldsymbol{0}$, such that $E_{\chi 0}$ corresponds to the position of the nodes in energy. As we explicitly verify in the Appendix F, the expression defined for $E_{\chi 0}$ in Eq. (D2) reproduces the expected result $E_{\chi 0} = -\chi\tilde{b}_0$.

2. The residues

For second order poles, the residue of $g^\chi_\rho(k_0, \boldsymbol{k})$ in the variable k_0 is

$$\text{Res}\left[g^\chi_\rho(k_0, \boldsymbol{k})\right] = \frac{d}{dk_0}\left[\left(k_0 - k_{0s}^{\chi\#}\right)^2 g^\chi_\rho(k_0, \boldsymbol{k})\right]\Big|_{k_0 = k_{0s}^{\chi\#}}, \qquad \text{(D3)}$$

where $k_{0s}^{\chi\#}$ denote the position of the poles, given by Eq. (D1). To proceed, we first write $g^\chi_\rho(k_0, \boldsymbol{k})$ as an explicit function of k_0 and k_i, i.e.,

$$g^\chi_\rho(k_0, \boldsymbol{k}) = \frac{[k_0 + (m_\chi)^j{}_0 k_j]\delta^0{}_\rho + (m_\chi)^i{}_i k_j\delta^i{}_\rho - (C_\chi)_\rho}{(k_0 - k_{0s}^{\chi\#})^2(k_0 - k_{0-s}^{\chi\#})^2}. \qquad \text{(D4)}$$

Calculating the residue yields

$$\text{Res}\left[g^\chi_\rho(k_0, \boldsymbol{k})\right] = \frac{d}{dk_0}\left\{\frac{[k_0 + (m_\chi)^j{}_0 k_j]\delta^0{}_\rho + (m_\chi)^j{}_i k_j\delta^i{}_\rho - (C_\chi)_\rho}{(k_0 - k_{0-s}^{\chi\#})^2}\right\}\Bigg|_{k_0 = k_{0s}^{\chi\#}}$$

$$= \delta^0{}_\rho\left[\frac{1}{(k_{0s}^{\chi\#} - k_{0-s}^{\chi\#})^2} - 2\frac{k_{0s}^{\chi\#} + (m_\chi)^j{}_0 k_j - (C_\chi)_0}{(k_{0s}^{\chi\#} - k_{0-s}^{\chi\#})^3}\right] - 2\delta^i{}_\rho\frac{(m_\chi)^j{}_i k_j - (C_\chi)_i}{(k_{0s}^{\chi\#} - k_{0-s}^{\chi\#})^3}. \qquad \text{(D5)}$$

However, from Eq. (D1) one finds

$$k_{0s}^{\chi\#} - k_{0-s}^{\chi\#} = 2s|\boldsymbol{k}' - \boldsymbol{C}_\chi|,$$
$$k_{0s}^{\chi\#} + (m_\chi)^j{}_0 k_j - (C_\chi)_0 = s|\boldsymbol{k}' - \boldsymbol{C}_\chi|, \qquad \text{(D6)}$$

and thus

$$\text{Res}\left[g^\chi_\rho(k_0, \boldsymbol{k})\right]$$
$$= \delta^0{}_\rho\left[\frac{1}{4|\boldsymbol{k}' - \boldsymbol{C}_\chi|^2} - 2\frac{s|\boldsymbol{k}' - \boldsymbol{C}_\chi|}{8s|\boldsymbol{k}' - \boldsymbol{C}_\chi|^3}\right] - 2\delta^i{}_\rho\frac{k'_i - (C_\chi)_i}{8s|\boldsymbol{k}' - \boldsymbol{C}_\chi|^3}$$
$$= -s\delta^i{}_\rho\frac{k'_i - (C_\chi)_i}{4|\boldsymbol{k}' - \boldsymbol{C}_\chi|^3}. \qquad \text{(D7)}$$

We observe that the residues have the monopole-like structure resembling the Berry curvature (67).

APPENDIX E: CALCULATION OF $I^{\chi s}$

In the main text we find twice the generic integral

$$\boldsymbol{I}^{\chi s} = \int \frac{d^3 q}{(2\pi)^3} \frac{\boldsymbol{q}}{|\boldsymbol{q}|^3} H(\mu - Q^s), \qquad \text{(E1)}$$

with $Q^s = \boldsymbol{W} \cdot \boldsymbol{q} + s|\boldsymbol{q}| + E_0$, where $s = \pm 1$ denotes the band index. The dependence of $\boldsymbol{I}^{\chi s}$ on the chirality χ is implicit in the vector $\boldsymbol{W}$, related to the tilting and the anisotropy, together with E_0 which determines the location in energy of each node. In the following we do not indicate the chirality index for simplicity in the notation. This integral naturally emerges when computing the μ-dependent contribution to the vacuum polarization tensor in Sec. IV B as well as in Sec. V when we evaluate the anomalous Hall current in a kinetic theory approach.

For the subsequent analyses we choose a spherical coordinate system with $\boldsymbol{W}$ pointing along the z-axis, such that $Q^s = s|\boldsymbol{q}|(1 + s|\boldsymbol{W}|\cos\theta) + E_0$. The Heaviside function H appearing in the integral (E1) imposes the restriction

$$\mu - E_0 > s|\boldsymbol{q}|(1 + s|\boldsymbol{W}|\cos\theta), \qquad \text{(E2)}$$

which requires some care for its implementation since it depends on the magnitude of $|\boldsymbol{W}|$. In this paper we consider the case $|\boldsymbol{W}| < 1$, which corresponds to a type-I WSM. With this choice, it is clear that $1 + s|\boldsymbol{W}|\cos\theta > 0$ for all values of θ, and hence the band index controls the sign of the right-hand side of Eq. (E2). On the other hand, the case

$|W| > 1$, which corresponds to a type-II WSM, presents additional difficulties since the right-hand side changes sign at $\theta = \arccos(-s/|W|)$ and make some integrals diverge, thus requiring to introduce additional cutoffs in the model. This case is beyond the scope of the present work. The simplest way of calculating the integral (E1) is to take advantage of the identity

$$\frac{\boldsymbol{q}}{|\boldsymbol{q}|^3} = -\nabla_q \frac{1}{|\boldsymbol{q}|}, \tag{E3}$$

and subsequently integrate by parts to obtain

$$\boldsymbol{I}^{\chi s} = -\int \frac{d^3\boldsymbol{q}}{(2\pi)^3} \left\{ \nabla_q \left[\frac{1}{|\boldsymbol{q}|} H(\mu - Q^s) \right] - \frac{1}{|\boldsymbol{q}|} \nabla_q H(\mu - Q^s) \right\}. \tag{E4}$$

Using the Gauss theorem, the first term (to be called $\boldsymbol{I}_S^{\chi s}$) yields the surface integral

$$\boldsymbol{I}_S^{\chi s} = -\lim_{|\boldsymbol{q}| \to \infty} \oint \frac{d\boldsymbol{S}}{(2\pi)^3} \frac{1}{|\boldsymbol{q}|} H(\mu - Q^s). \tag{E5}$$

To evaluate this integral we choose a spherical-shaped surface centered at the origin such that $d\boldsymbol{S} = \hat{\boldsymbol{q}} d\Omega$, where $d\Omega = \sin\theta d\theta d\phi$ is the differential of solid angle. Besides, we observe that we require the limit of the Heaviside function when $|\boldsymbol{q}| \to \infty$. For type-I WSMs ($|W| < 1$) we find

$$\lim_{|\boldsymbol{q}| \to \infty} H(\mu - Q^s) = H(-s), \tag{E6}$$

since $1 + s|W|\cos\theta > 0$ for all values of θ. This makes the integrand of Eq. (E5) independent of the angular variables, thus implying

$$\boldsymbol{I}_S^{\chi s} = -H(-s) \oint \frac{d\Omega}{(2\pi)^3} \frac{\hat{\boldsymbol{q}}}{|\boldsymbol{q}|} = 0. \tag{E7}$$

Thus we are left with the second term of Eq. (E4), which we rewrite as follows:

$$\begin{aligned} \boldsymbol{I}^{\chi s} &= \int \frac{d^3\boldsymbol{q}}{(2\pi)^3} \frac{1}{|\boldsymbol{q}|} \nabla_q H(\mu - Q^s) \\ &= -\int \frac{d^3\boldsymbol{q}}{(2\pi)^3} \frac{\nabla_q Q^s}{|\boldsymbol{q}|} \delta(\mu - Q^s). \end{aligned} \tag{E8}$$

Now, using the fact that $\nabla_q Q^s = \boldsymbol{W} + s\hat{\boldsymbol{q}}$ and introducing $\Lambda \equiv \mu - E_0$, we obtain

$$\boldsymbol{I}^{\chi s} = -\int \frac{d^3\boldsymbol{q}}{(2\pi)^3} \frac{\boldsymbol{W} + s\hat{\boldsymbol{q}}}{|\boldsymbol{q}|} \delta[\Lambda - s|\boldsymbol{q}|(1 + s\boldsymbol{W} \cdot \hat{\boldsymbol{q}})]. \tag{E9}$$

Since the only vector at our disposal is $\boldsymbol{W}$ we have $\boldsymbol{I}^{\chi s} = M^{\chi s}\boldsymbol{W}$, where

$$M^{\chi s} = -\frac{1}{W^2} \int \frac{d^3\boldsymbol{q}}{(2\pi)^3} \frac{\boldsymbol{W} \cdot (\boldsymbol{W} + s\hat{\boldsymbol{q}})}{|\boldsymbol{q}|} \delta[\Lambda - s|\boldsymbol{q}|(1 + s\boldsymbol{W} \cdot \hat{\boldsymbol{q}})]. \tag{E10}$$

To evaluate this integral we employ a spherical coordinate system with $\boldsymbol{W}$ pointing along the z-axis. The radial integral can be performed by decomposing the Dirac delta as

$$\delta[\Lambda - s|\boldsymbol{q}|(1 + s\boldsymbol{W} \cdot \hat{\boldsymbol{q}})] = \frac{\delta(|\boldsymbol{q}| - q^*)}{|1 + s\boldsymbol{W} \cdot \hat{\boldsymbol{q}}|} H(q^*), \tag{E11}$$

where

$$q^* = \frac{s\Lambda}{1 + s\boldsymbol{W} \cdot \hat{\boldsymbol{q}}}. \tag{E12}$$

Note that the Heaviside function in Eq. (E11) guarantees that the root (E12) should be positive. The case at hand is simple since $|W| < 1$ implies $1 + s\boldsymbol{W} \cdot \hat{\boldsymbol{q}} > 0$ and therefore the Heaviside function in (E11) restricts the product $s\Lambda$ to be positive. Therefore, performing the radial integration in (E10) we obtain

$$M^{\chi s} = -\frac{s\Lambda}{|W|} H(s\Lambda) \int \frac{d\Omega}{(2\pi)^3} \frac{|W| + s\cos\theta}{(1 + s|W|\cos\theta)^2}. \tag{E13}$$

This integral can be easily computed with a simple change of variables. The final result is

$$M^{\chi s} = \frac{s\Lambda}{2\pi^2 |W|^3} H(s\Lambda) \quad (|W| - \operatorname{arctanh}|W|), \tag{E14}$$

such that $\boldsymbol{I}^{\chi s} = M^{\chi s}\boldsymbol{W}$.

APPENDIX F: THE VECTOR $\mathcal{B}_\lambda$

Following Eqs. (13) and (14) we realize that the effective action is determined by the vector $\mathcal{B}_\lambda$, which has a contribution given by Eq. (43), to be called universal for the reasons indicated after obtaining $\mathcal{B}_\lambda^{(1)}$ in this section, together with a correction term due to finite density given by Eq. (62). Our Eqs. (43) and (62) are expressed in terms of the parameters of the SME. The goal of this section is to rewrite the vector $\mathcal{B}_\lambda$ in terms of the parameters describing the condensed matter Hamiltonian (30).

Our first task is to compute the inverse of the matrix $(m_\chi)^\mu{}_\nu$. To this end we use the representation (36) together with the equivalences in Eq. (39). In this case, the matrix $[(m_\chi)^\mu{}_\nu]$ can be written as

$$[(m_\chi)^\mu{}_\nu] \equiv \begin{pmatrix} 1 & 0 \\ \boldsymbol{v}_\chi & \mathbb{A}_\chi \end{pmatrix}, \qquad \mathbb{A}_\chi = [(A_\chi)_{ij}], \tag{F1}$$

such that the inverse is given by

$$[(m_\chi^{-1})^\mu{}_\nu] \equiv \begin{pmatrix} 1 & 0 \\ -\mathbb{A}_\chi^{-1}\mathbf{v}_\chi & \mathbb{A}_\chi^{-1} \end{pmatrix}, \qquad (A_\chi)_{ij}(A_\chi^{-1})_{jk} = \delta_{ik}.$$

$$\text{(F2)}$$

Therefore, the required components (i.e., space-time and space-space) of this matrix become

$$(m_\chi^{-1})^i{}_0 = -[\mathbb{A}_\chi^{-1}\mathbf{v}_\chi]_i = -(A_\chi^{-1})_{ij}v_\chi^j, \qquad (m_\chi^{-1})^i{}_j = (A_\chi^{-1})_{ij}.$$

$$\text{(F3)}$$

Besides the above inverses we also need $\mathcal{V}^i$, which is given by Eq. (53). Note that $\mathcal{V}^i$ yields N_χ in Eq. (60). Substituting Eqs. (F1) and (F3) into Eq. (53) we obtain

$$\mathcal{V}_\chi{}^j = (m_\chi^{-1})^j{}_i(m_\chi)^i{}_0 = (A_\chi^{-1})_{ji}v_\chi^i. \qquad \text{(F4)}$$

Now we have the missing ingredients to establish the correspondence between the SME coefficients with the parameters appearing in the condensed matter Hamiltonian (30).

On the one hand, using $(C_\chi)_0 = \chi(v_\chi^i\tilde{b}^i - \tilde{b}_0)$ and $(C_\chi)_j = \chi\tilde{b}^i(A_\chi)_{ij}$ defined by Eq. (39), we compute the vector $\mathcal{B}_\lambda^{(1)}$ given by Eq. (43) which determines the universal contribution. Taking our choice $N = -1/(8\pi^2)$ the time component becomes

$$\mathcal{B}_0^{(1)} = -\frac{1}{2}\sum_{\chi=\pm 1}\chi\left[(C_\chi)_0(m_\chi^{-1})^0{}_0 + (C_\chi)_j(m_\chi^{-1})^j{}_0\right]$$

$$= -\frac{1}{2}\sum_{\chi=\pm 1}\chi\left[\chi(v_\chi^i\tilde{b}^i - \tilde{b}_0) - \chi\tilde{b}^i(A_\chi)_{ij}(A_\chi^{-1})_{jk}v_\chi^k\right]$$

$$= -\frac{1}{2}\sum_{\chi=\pm 1}\left[(v_\chi^i\tilde{b}^i - \tilde{b}_0) - \tilde{b}^iv_\chi^i\right] = \tilde{b}_0, \qquad \text{(F5)}$$

while the space-component simplifies to

$$\mathcal{B}_i^{(1)} = -\frac{1}{2}\sum_{\chi=\pm 1}\chi\left[(C_\chi)_0(m_\chi^{-1})^0{}_i + (C_\chi)_j(m_\chi^{-1})^j{}_i\right]$$

$$= -\frac{1}{2}\sum_{\chi=\pm 1}\chi\left[0 + \chi\tilde{b}^k(A_\chi)_{kj}(A_\chi^{-1})_{ji}\right]$$

$$= -\frac{1}{2}\sum_{\chi=\pm 1}\tilde{b}^i = \tilde{b}_i. \qquad \text{(F6)}$$

Note that $\mathcal{B}_\lambda^{(1)}$ depends only upon the position of the Weyl nodes in momentum and energy, and in this sense we call this contribution universal, since it becomes independent of the anisotropy, tilting and chemical potential.

On the other hand, using Eq. (F4) we obtain

$$E_{\chi 0} = \mathcal{V}_\chi \cdot \mathbf{C}_\chi + (C_\chi)_0$$

$$= (A_\chi^{-1})_{ji}v_\chi^i\left[\chi\tilde{b}^k(A_\chi)_{kj}\right] + \chi(v_\chi^i\tilde{b}^i - \tilde{b}_0)$$

$$= -\chi\tilde{b}_0, \qquad \text{(F7)}$$

such that $\Lambda_\chi = \mu + \chi\tilde{b}_0$. This is a measure of the position of the nodes with respect to the chemical potential. Now, we evaluate the components of the vector $\mathcal{B}_\lambda^{(2)}$, given by Eq. (62), which determines the μ-dependent contribution. The time component becomes

$$\mathcal{B}_0^{(2)} = -\sum_{\chi=\pm 1}\chi\Lambda_\chi N_\chi(m_\chi^{-1})^j{}_0(\mathcal{V}_\chi)_j$$

$$= -\sum_{\chi=\pm 1}\chi\Lambda_\chi N_\chi\left[-(A_\chi^{-1})_{ji}v_\chi^i\right]\left[(-A_\chi^{-1})_{jk}v_\chi^k\right]$$

$$= -\sum_{\chi=\pm 1}\chi\Lambda_\chi N_\chi\mathbf{v}_\chi(\mathbb{A}_\chi^{-1})^T\mathbb{A}_\chi^{-1}\mathbf{v}_\chi, \qquad \text{(F8)}$$

while the space-component simplifies to

$$\mathcal{B}_i^{(2)} = -\sum_{\chi=\pm 1}\chi\Lambda_\chi N_\chi(m_\chi^{-1})^j{}_i(\mathcal{V}_\chi)_j$$

$$= -\sum_{\chi=\pm 1}\chi\Lambda_\chi N_\chi(A_\chi^{-1})_{ji}\left[-(A_\chi^{-1})_{jk}v_\chi^k\right]$$

$$= +\sum_{\chi=\pm 1}\chi\Lambda_\chi N_\chi\left[(\mathbb{A}_\chi^{-1})^T\mathbb{A}_\chi^{-1}\mathbf{v}_\chi\right]_i. \qquad \text{(F9)}$$

In these expressions

$$N_\chi = \frac{1}{2|\mathcal{V}_\chi|^3}\left(|\mathcal{V}_\chi| - \text{arctanh}(|\mathcal{V}_\chi|)\right), \qquad \text{(F10)}$$

where $\mathcal{V}_\chi = \mathbb{A}_\chi^{-1}\mathbf{v}_\chi$. All in all, we have obtained the full characterization of the effective action $S_{\text{eff}}^{(2)}(A)$ given by Eq. (13) in terms of the polarization tensor $\Pi^{\mu\nu}$ defined by Eq. (14), with the vector $\mathcal{B}_\lambda$ written in terms of the parameters of the Hamiltonian of the WSM (30).

Summarizing, the results are

$$\mathcal{B}_0 = \tilde{b}_0 - \sum_{\chi=\pm 1}\chi\Lambda_\chi N_\chi\mathbf{v}_\chi(\mathbb{A}_\chi^{-1})^T(\mathbb{A}_\chi^{-1})\mathbf{v}_\chi,$$

$$\mathcal{B}_k = \tilde{b}_k + \sum_{\chi=\pm 1}\chi\Lambda_\chi N_\chi\left[(\mathbb{A}_\chi^{-1})^T(\mathbb{A}_\chi^{-1})\mathbf{v}_\chi\right]_k,$$

$$\Lambda_\chi = \mu + \chi\tilde{b}_0, \qquad \mathcal{V}_\chi = \mathbb{A}_\chi^{-1}\mathbf{v}_\chi,$$

$$N_\chi = \frac{1}{2|\mathcal{V}_\chi|^3}\left(|\mathcal{V}_\chi| - \text{arctanh}(|\mathcal{V}_\chi|)\right). \qquad \text{(F11)}$$

[1] W. Dittrich and H. Gies, *Probing the Quantum Vacuum. Perturbative Effective Action Approach in Quantum Electrodynamics and Its Application* (Springer, Berlin, Heidelberg, 2000), Vol. 166.

[2] W. Dittrich and M. Reuter, *Effective Lagrangians in Quantum Electrodynamics* (Springer-Verlag, Berlin, 1985), Vol. 220.

[3] W. Heisenberg and H. Euler, Consequences of Dirac's theory of positrons, Z. Phys. **98,** 714 (1936).

[4] H. Euler and B. Kockel, The scattering of light by light in Dirac's theory, Naturwissenschaften **23,** 246 (1935).

[5] R. Karplus and M. Neuman, The scattering of light by light, Phys. Rev. **83,** 776 (1951).

[6] F. Sauter, Uber das Verhalten eines Elektrons im homogenen elektrischen Feld nach der relativistischen Theorie Diracs, Z. Phys. **69,** 742 (1931).

[7] J. S. Schwinger, On gauge invariance and vacuum polarization, Phys. Rev. **82,** 664 (1951).

[8] J. Schwinger, The theory of quantized fields. V, Phys. Rev. **93,** 615 (1954).

[9] J. Schwinger, The theory of quantized fields. VI, Phys. Rev. **94,** 1362 (1954).

[10] G. V. Dunne, Heisenberg-Euler effective Lagrangians: Basics and extensions, in *From Fields to Strings: Circumnavigating Theoretical Physics*, edited by M. Shifman, A. Vainshtein, and J. Wheater (World Scientific, Singapore, 2004), pp. 445–522.

[11] V. B. Berestetskii, E. M. Lifshitz, and L. P. Pitaevskii, *Quantum Electrodynamics*, Course of Theoretical Physics Vol. 4 (Pergamon Press, Oxford, 1982).

[12] N. B. Narozhnyi and A. I. Nikishov, The simplest processes in the pair creating electric field, Yad. Fiz. **11,** 1072 (1970).

[13] C. Martin and D. Vautherin, Finite-size effects in pair production by an external field, Phys. Rev. D **40,** 1667 (1989).

[14] G. V. Dunne and T. M. Hall, An exact $(3 + 1)$-dimensional QED effective action, Phys. Lett. B **419,** 322 (1998).

[15] G. V. Dunne and T. Hall, On the QED effective action in time dependent electric backgrounds, Phys. Rev. D **58,** 105022 (1998).

[16] A. Chodos, K. Everding, and D. A. Owen, QED with a chemical potential: 1. The case of a constant magnetic field, Phys. Rev. D **42,** 2881 (1990).

[17] H. A. Weldon, Covariant calculations at finite temperature: The relativistic plasma, Phys. Rev. D **26,** 1394 (1982).

[18] K. Ahmed and S. S. Masood, Vacuum polarization at finite temperature and density in QED, Ann. Phys. (N.Y.) **207,** 460 (1991).

[19] M. Le Bellac, *Thermal Field Theory*, Cambridge Monographs on Mathematical Physics (Cambridge University Press, Cambridge, England, 1996).

[20] J. I. Kapusta and C. Gale, *Finite-Temperature Field Theory: Principles and Applications*, Cambridge Monographs on Mathematical Physics (Cambridge University Press, Cambridge, England, 2011).

[21] W. Dittrich, Effective Lagragians at finite temperature, Phys. Rev. D **19,** 2385 (1979).

[22] C. W. Bernard, Feynman rules for gauge theories at finite temperature, Phys. Rev. D **9,** 3312 (1974).

[23] A. K. Das, *Finite Temperature Field Theory* (World Scientific, New York, 1997).

[24] *Statistical Mechanics: An Advanced Course with Problems and Solutions*, edited by R. Kubo, 2nd ed., North-Holland Personal Library (North-Holland, Amsterdam, 1999).

[25] M. G. Mustafa, An introduction to thermal field theory and some of its application, Eur. Phys. J. Spec. Top. **232,** 1369 (2023).

[26] A. Fedotov, A. Ilderton, F. Karbstein, B. King, D. Seipt, H. Taya, and G. Torgrimsson, Advances in QED with intense background fields, Phys. Rep. **1010,** 1 (2023).

[27] C. Schubert, Perturbative quantum field theory in the string inspired formalism, Phys. Rep. **355,** 73 (2001).

[28] C. Schubert, The worldline formalism in strong-field QED, J. Phys. Conf. Ser. **2494,** 012020 (2023).

[29] D. Colladay and V. A. Kostelecký, *CPT* violation and the standard model, Phys. Rev. D **55,** 6760 (1997).

[30] D. Colladay and V. A. Kostelecký, Lorentz-violating extension of the standard model, Phys. Rev. D **58,** 116002 (1998).

[31] S. M. Carroll, G. B. Field, and R. Jackiw, Limits on a Lorentz- and parity-violating modification of electrodynamics, Phys. Rev. D **41,** 1231 (1990).

[32] R. D. Peccei and H. R. Quinn, *CP* conservation in the presence of instantons, Phys. Rev. Lett. **38,** 1440 (1977).

[33] P. Sikivie, Experimental tests of the invisible axion, Phys. Rev. Lett. **51,** 1415 (1983); **52,** 695(E) (1984).

[34] R. Jackiw and V. A. Kostelecky, Radiatively induced Lorentz and *CPT* violation in electrodynamics, Phys. Rev. Lett. **82,** 3572 (1999).

[35] M. Pérez-Victoria, Exact calculation of the radiatively induced Lorentz and *CPT* violation in QED, Phys. Rev. Lett. **83,** 2518 (1999).

[36] O. A. Battistel and G. Dallabona, Role of ambiguities and gauge invariance in the calculation of the radiatively induced Chern-Simons shift in extended QED, J. Phys. G **27,** L53 (2001).

[37] M. Perez-Victoria, Physical (ir)relevance of ambiguities to Lorentz and *CPT* violation in QED, J. High Energy Phys. 04 (2001) 032.

[38] A. A. Andrianov, P. Giacconi, and R. Soldati, Lorentz and *CPT* violations from Chern-Simons modifications of QED, J. High Energy Phys. 02 (2002) 030.

[39] B. Altschul, Failure of gauge invariance in the nonperturbative formulation of massless Lorentz violating QED, Phys. Rev. D **69,** 125009 (2004).

[40] B. Altschul, Gauge invariance and the Pauli-Villars regulator in Lorentz- and *CPT*-violating electrodynamics, Phys. Rev. D **70,** 101701 (2004).

[41] J. Alfaro, A. A. Andrianov, M. Cambiaso, P. Giacconi, and R. Soldati, Bare and induced Lorentz and *CPT* invariance violations in QED, Int. J. Mod. Phys. A **25,** 3271 (2010).

[42] R. Jackiw, When radiative corrections are finite but undetermined, Int. J. Mod. Phys. B **14,** 2011 (2000).

[43] B. Altschul, There is no ambiguity in the radiatively induced gravitational Chern-Simons term, Phys. Rev. D **99,** 125009 (2019).

[44] J. Furtado and T. Mariz, Lorentz-violating Euler-Heisenberg effective action, Phys. Rev. D **89**, 025021 (2014).

[45] T. Mariz, J. R. Nascimento, A. Y. Petrov, L. Y. Santos, and A. J. da Silva, Lorentz violation and the proper-time method, Phys. Lett. B **661**, 312 (2008).

[46] A. F. Ferrari, J. Furtado, J. F. Assunção, T. Mariz, and A. Y. Petrov, One-loop calculations in Lorentz-breaking theories and proper-time method, Europhys. Lett. **136**, 21002 (2021).

[47] T. Mariz, R. V. Maluf, J. R. Nascimento, and A. Y. Petrov, On one-loop corrections to the *CPT*-even Lorentz-breaking extension of QED, Int. J. Mod. Phys. A **33**, 1850018 (2018).

[48] M. A. Anacleto, F. A. Brito, O. Holanda, and E. Passos, Induction of the Lorentz-violating effective actions in quantum electrodynamics, Int. J. Mod. Phys. A **32**, 1750128 (2017).

[49] A. P. Baeta Scarpelli, T. Mariz, J. R. Nascimento, and A. Y. Petrov, Four-dimensional aether-like Lorentz-breaking QED revisited and problem of ambiguities, Eur. Phys. J. C **73**, 2526 (2013).

[50] R. Casana, M. M. Ferreira, Jr., R. V. Maluf, and F. E. P. dos Santos, Radiative generation of the *CPT*-even gauge term of the SME from a dimension-five nonminimal coupling term, Phys. Lett. B **726**, 815 (2013).

[51] M. Gomes, J. R. Nascimento, A. Y. Petrov, and A. J. da Silva, On the aether-like Lorentz-breaking actions, Phys. Rev. D **81**, 045018 (2010).

[52] T. Mariz, Radiatively induced Lorentz-violating operator of mass dimension five in QED, Phys. Rev. D **83**, 045018 (2011).

[53] T. Mariz, J. R. Nascimento, and A. Y. Petrov, On the perturbative generation of the higher-derivative Lorentz-breaking terms, Phys. Rev. D **85**, 125003 (2012).

[54] L. H. C. Borges, A. G. Dias, A. F. Ferrari, J. R. Nascimento, and A. Y. Petrov, Generation of higher derivatives operators and electromagnetic wave propagation in a Lorentz-violation scenario, Phys. Lett. B **756**, 332 (2016).

[55] A. P. Baeta Scarpelli, L. C. T. Brito, J. C. C. Felipe, J. R. Nascimento, and A. Y. Petrov, Higher-order one-loop contributions in Lorentz-breaking QED, Europhys. Lett. **123**, 21001 (2018).

[56] A. F. Ferrari, J. R. Nascimento, and A. Y. Petrov, Radiative corrections and Lorentz violation, Eur. Phys. J. C **80**, 459 (2020).

[57] A. G. Grushin, Consequences of a condensed matter realization of Lorentz violating QED in Weyl semi-metals, Phys. Rev. D **86**, 045001 (2012).

[58] V. A. Kostelecký, in Concepts in Lorentz and *CPT* violation, edited by R. Lehnert (World Scientific, Singapore, 2022).

[59] N. McGinnis, Transport phenomena in Weyl semimetals from effective actions of the standard-model extension, in *CPT and Lorentz Symmetry* (World Scientific, Singapore, 2023).

[60] L. F. Urrutia, LIV in matter, in *CPT and Lorentz Symmetry* (World Scientific, Singapore, 2023).

[61] A. Gómez, A. Martín-Ruiz, and L. F. Urrutia, Effective electromagnetic actions for Lorentz violating theories exhibiting the axial anomaly, Phys. Lett. B **829**, 137043 (2022).

[62] V. A. Kostelecký, R. Lehnert, N. McGinnis, M. Schreck, and B. Seradjeh, Lorentz violation in Dirac and Weyl semimetals, Phys. Rev. Res. **4**, 023106 (2022).

[63] M. M. Vazifeh and M. Franz, Electromagnetic response of Weyl semimetals, Phys. Rev. Lett. **111**, 027201 (2013).

[64] N. P. Armitage, E. J. Mele, and A. Vishwanath, Weyl and Dirac semimetals in three dimensional solids, Rev. Mod. Phys. **90**, 015001 (2018).

[65] B. Yan and C. Felser, Topological materials: Weyl semimetals, Annu. Rev. Condens. Matter Phys. **8**, 337 (2017).

[66] H. B. Nielsen and M. Ninomiya, Adler-Bell-Jackiw anomaly and Weyl fermions in crystal, Phys. Lett. B **130**, 389 (1983).

[67] S.-M. Huang, S.-Y. Xu, I. Belopolski, C.-C. Lee, G. Chang, B. Wang, N. Alidoust, G. Bian, M. Neupane, C. Zhang, S. Jia, A. Bansil, H. Lin, and M. Z. Hasan, A Weyl fermion semimetal with surface Fermi arcs in the transition metal monopnictide TaAs class, Nat. Commun. **6**, 7373 (2015).

[68] H. Weng, C. Fang, Z. Fang, B. A. Bernevig, and X. Dai, Weyl semimetal phase in noncentrosymmetric transition-metal monophosphides, Phys. Rev. X **5**, 011029 (2015).

[69] S.-Y. Xu *et al.*, Discovery of a Weyl fermion semimetal and topological Fermi arcs, Science **349**, 613 (2015).

[70] L. Lu, Z. Wang, D. Ye, L. Ran, L. Fu, J. D. Joannopoulos, and M. Soljačić, Experimental observation of Weyl points, Science **349**, 622 (2015).

[71] B. Q. Lv, H. M. Weng, B. B. Fu, X. P. Wang, H. Miao, J. Ma, P. Richard, X. C. Huang, L. X. Zhao, G. F. Chen, Z. Fang, X. Dai, T. Qian, and H. Ding, Experimental discovery of Weyl semimetal TaAs, Phys. Rev. X **5**, 031013 (2015).

[72] B. Q. Lv, S. Muff, T. Qian, Z. D. Song, S. M. Nie, N. Xu, P. Richard, C. E. Matt, N. C. Plumb, L. X. Zhao, G. F. Chen, Z. Fang, X. Dai, J. H. Dil, J. Mesot, M. Shi, H. M. Weng, and H. Ding, Observation of Fermi-arc spin texture in TaAs, Phys. Rev. Lett. **115**, 217601 (2015).

[73] S.-Y. Xu *et al.*, Discovery of a Weyl fermion state with Fermi arcs in niobium arsenide, Nat. Phys. **11**, 748 (2015).

[74] B. Q. Lv, N. Xu, H. M. Weng, J. Z. Ma, P. Richard, X. C. Huang, L. X. Zhao, G. F. Chen, C. E. Matt, F. Bisti, V. N. Strocov, J. Mesot, Z. Fang, X. Dai, T. Qian, M. Shi, and H. Ding, Observation of Weyl nodes in TaAs, Nat. Phys. **11**, 724 (2015).

[75] Z. K. Liu, L. X. Yang, Y. Sun, T. Zhang, H. Peng, H. F. Yang, C. Chen, Y. Zhang, Y. F. Guo, D. Prabhakaran, M. Schmidt, Z. Hussain, S. K. Mo, C. Felser, B. Yan, and Y. L. Chen, Evolution of the Fermi surface of Weyl semimetals in the transition metal pnictide family, Nat. Mater. **15**, 27 (2016).

[76] X. Wan, A. M. Turner, A. Vishwanath, and S. Y. Savrasov, Topological semimetal and Fermi-arc surface states in the electronic structure of pyrochlore iridates, Phys. Rev. B **83**, 205101 (2011).

[77] W. Witczak-Krempa and Y. B. Kim, Topological and magnetic phases of interacting electrons in the pyrochlore iridates, Phys. Rev. B **85**, 045124 (2012).

[78] G. Chen and M. Hermele, Magnetic orders and topological phases from f-d exchange in pyrochlore iridates, Phys. Rev. B **86**, 235129 (2012).

[79] S.-Y. Xu *et al.*, Spin polarization and texture of the Fermi arcs in the Weyl fermion semimetal TaAs, Phys. Rev. Lett. **116**, 096801 (2016).

[80] R. Kubo, Statistical-mechanical theory of irreversible processes. I. General theory and simple applications to magnetic and conduction problems, J. Phys. Soc. Jpn. **12**, 570 (1957).

[81] M. A. Stephanov and Y. Yin, Chiral kinetic theory, Phys. Rev. Lett. **109**, 162001 (2012).

[82] A. A. Zyuzin and A. A. Burkov, Topological response in Weyl semimetals and the chiral anomaly, Phys. Rev. B **86**, 115133 (2012).

[83] K. Fujikawa and H. Suzuki, *Path Integrals and Quantum Anomalies*, International Series of Monographs on Physics (Clarendon Press, Oxford, 2004).

[84] R. Bertlmann, *Anomalies in Quantum Field Theory*, International Series of Monographs on Physics (Clarendon Press, New York, 2000).

[85] P. Goswami and S. Tewari, Axionic field theory of $(3 + 1)$-dimensional Weyl semimetals, Phys. Rev. B **88**, 245107 (2013).

[86] A. Sekine and K. Nomura, Axion electrodynamics in topological materials, J. Appl. Phys. **129**, 141101 (2021).

[87] M. N. Chernodub, Y. Ferreiros, A. G. Grushin, K. Landsteiner, and M. A. H. Vozmediano, Thermal transport, geometry, and anomalies, Phys. Rep. **977**, 1 (2022).

[88] P. Arias, H. Falomir, J. Gamboa, F. Mendez, and F. A. Schaposnik, Chiral anomaly beyond Lorentz invariance, Phys. Rev. D **76**, 025019 (2007).

[89] A. Salvio, Relaxing Lorentz invariance in general perturbative anomalies, Phys. Rev. D **78**, 085023 (2008).

[90] A. P. Baeta Scarpelli, T. Mariz, J. R. Nascimento, and A. Y. Petrov, On the anomalies in Lorentz-breaking theories, Int. J. Mod. Phys. A **31**, 1650063 (2016); **32**, 1792002(E) (2017).

[91] A. Gómez and L. Urrutia, The axial anomaly in Lorentz violating theories: Towards the electromagnetic response of weakly tilted Weyl semimetals, Symmetry **13**, 1181 (2021).

[92] V. A. Kostelecký and N. Russell, Data tables for Lorentz and *CPT* violation, Rev. Mod. Phys. **83**, 11 (2011).

[93] J. D. Jackson, *Classical electrodynamics*, 3rd ed. (Wiley, New York, NY, 1999).

[94] A. P. B. Scarpelli, M. Sampaio, M. C. Nemes, and B. Hiller, Gauge invariance and the *CPT* and Lorentz violating induced Chern–Simons-like term in extended QED, Eur. Phys. J. C **56**, 571 (2008).

[95] D. Xiao, M.-C. Chang, and Q. Niu, Berry phase effects on electronic properties, Rev. Mod. Phys. **82**, 1959 (2010).

[96] D. Xiao, W. Yao, and Q. Niu, Valley-contrasting physics in graphene: Magnetic moment and topological transport, Phys. Rev. Lett. **99**, 236809 (2007).

[97] R. Karplus and J. M. Luttinger, Hall effect in ferromagnetics, Phys. Rev. **95**, 1154 (1954).

[98] N. Nagaosa, J. Sinova, S. Onoda, A. H. MacDonald, and N. P. Ong, Anomalous Hall effect, Rev. Mod. Phys. **82**, 1539 (2010).

[99] A. A. Burkov, Anomalous Hall effect in Weyl metals, Phys. Rev. Lett. **113**, 187202 (2014).

[100] J.-R. Soh, F. de Juan, M. G. Vergniory, N. B. M. Schröter, M. C. Rahn, D. Y. Yan, J. Jiang, M. Bristow, P. Reiss, J. N. Blandy, Y. F. Guo, Y. G. Shi, T. K. Kim, A. McCollam, S. H. Simon, Y. Chen, A. I. Coldea, and A. T. Boothroyd, Ideal Weyl semimetal induced by magnetic exchange, Phys. Rev. B **100**, 201102 (2019).

[101] D. Grassano, O. Pulci, E. Cannuccia, and F. Bechstedt, Influence of anisotropy, tilt and pairing of Weyl nodes: The Weyl semimetals TaAs, TaP, NbAs and NbP, Eur. Phys. J. B **93**, 157 (2020).